https://doi.org/10.5194/egusphere-2025-3423
Preprint. Discussion started: 15 September 2025

Exceptional high AOD over Svalbard in Summer 2019: A multi-instrumental approach

Sara Herrero-Anta[1, 2], Sabine Eckhardt[3], Nikolaos Evangeliou[3], Stefania Gilardoni[4], Sandra Graßl[5, 6], Dominic Heslin-Rees[7], Stelios Kazadzis[8], Natalia Kouremeti[8], Radovan Krejci[7], David Mateos[1, 2], Mauro Mazzola[4], Christoph Ritter[6], Roberto Román[1, 2], Kerstin Stebel[3], and Tymon Zielinski[9]

[1]Group of Atmospheric Optics, Universidad de Valladolid, Valladolid, 47011, Spain
[2]Laboratory of Disruptive Interdisciplinary Science (LaDIS), Universidad de Valladolid, Valladolid, 47011, Spain
[3]NILU, Kjeller, 2007, Norway
[4]National Research Council, Institute of Polar Science (CNR-ISP), Bologna, 40129, Italy
[5]Institute of Physics and Astronomy, University of Potsdam, Potsdam, 14476, Germany
[6]Alfred-Wegener-Institute Helmholtz Centre for Polar and Marine Research, Potsdam, 14473, Germany
[7]Department of of Environmental Science, Stockholm University, Stockholm, S10691, Sweden
[8]Physikalisch-Meteorologisches Observatorium Davos/World Radiation Centre (PMOD/WRC), Davos, 7260, Switzerland
[9]Polish Academy of Sciences, Institute of Oceanology, Sopot, 81-712, Poland

Correspondence: Sara Herrero-Anta (sara@goa.uva.es)

Abstract. In the summer of 2019, the Arctic region registered exceptionally high aerosol optical depth (AOD) values over Svalbard, linked to intense biomass burning (BB) and volcanic activity across the Northern Hemisphere. This study presents a comprehensive, multi-instrumental analysis of the aerosol conditions in and around Ny-Ålesund (Spitsbergen, Norway), combining data from ground-based sun-photometry, in-situ observations, active remote sensing (ground-based and on satellite), and atmospheric dispersion modeling (FLEXPART). Despite high AOD was observed during all the period, three different aerosol events are identified in the atmospheric column (6–10 July, 25–28 July, and 6–17 August). In contrast, in-situ surface stations only recorded significant aerosol load during 5–9 July, 30 August, and 12 September, suggesting that most of the aerosol particles remained above the boundary layer. Lidar and photometric observations revealed the presence of spherical, weakly absorbing Accumulation-mode particles (0.1-0.2 μm) in both the troposphere and stratosphere, with persistent layers extending above 10 km. Simulations carried out with FLEXPART correlate well with the measurements, attributing the observed aerosol events to multiple sources, including Siberian and North American wildfires, the Raikoke (Russia) volcanic eruption, and anthropogenic pollution. Overall, the aerosol radiative impact during this long-lasting event was substantial, with a mean reduction in direct solar radiation of approximately -74 W/m^2 during July and August. This work shows how the use of dispersion modelling together with multiple observation sources allows to achieve a more complete description of the atmospheric aerosol events and contributes to a better understanding of the overall picture.

1 Introduction

The Polar regions constitute sensitive habitats with a vulnerable climate; the particular characteristics of these areas determine the occurrence of feedback mechanisms that cause an accelerated rate of warming, known as polar amplification (Serreze and

https://doi.org/10.5194/egusphere-2025-3423
Preprint. Discussion started: 15 September 2025

Barry, 2011; Wendisch et al., 2023). The Arctic has been warming nearly four times faster than the globe since 1979 (Rantanen et al., 2022). This change in climate has an impact in the sources as well as the sinks of aerosols (Willis et al., 2018); therefore it is necessary to characterize and understand well the role of natural and anthropogenic pollutants in this region (Schmale et al., 2021).

In the Arctic, during summer, the aerosol particles typically present smaller sizes and a more local origin (Tunved et al., 2013a; Schmale et al., 2022; Graßl et al., 2024). However, biomass burning (BB) aerosol from forest fires can be transported from lower latitudes (Law and Stohl, 2007; Zielinski et al., 2020). In addition, volcanic eruptions can also sporadically increase the aerosol concentration in the high Arctic both at ground (Wittmann et al., 2017) and in elevated atmospheric layers (Cheremisin et al., 2019). Aerosol events can occur in the Arctic at any season (e.g. Warneke et al., 2010), but summer events are specially important for the surface energy budget, since they are characterized by higher solar radiation levels.Lisok et al. (2018) and Calì Quaglia et al. (2022) derived large negative radiative forcing of BB aerosol for the Arctic during summer events.

In recent years, a large effort has been conducted to monitoring aerosol particles over the Arctic through the deployment of instrumentation based on different measurement principles, as well as satellite missions. To consolidate all available information to date, in and around the Arctic region of Svalbard, the ReHearsol project (Re-evaluation and Homogenization of Aerosol Optical Depth Observations in Svalbard; Hansen et al., 2022), collected, integrated and analyzed observations of climate-relevant aerosol parameters like aerosol optical depth (AOD), Ångström exponent (AE) and black carbon (BC), among others. The outcome of this project was an integrated dataset for the years 2002-2020, which was analyzed in detail by Hansen et al. (2022) and Hansen et al. (2023). In adition, Xian et al. (2022b) and Xian et al. (2022a) combined AOD measurements from multi-agency aerosol reanalyses, remote-sensing retrievals, and ground observations available in the Arctic to analyze the climatology, trends and statistics of extreme events during the 2003-2019 period. This analysis showed an increase of the maximum AOD values in 2010–2019 compared to 2003–2009, related to stronger wildfire events in the recent years. In particular, it can be seen in the ReHeaersol dataset that the summer of 2019 clearly stands out, showing much higher AOD levels than any other period.

The summer of 2019 was a particularly intense fire season in the Northern Hemisphere, mainly due to large wildfires in North America and Siberia (Fazel-Rastgar and Sivakumar, 2022; Kharuk et al., 2022; CAMS, 2020; Johnson et al., 2021; Voronova et al., 2020). In addition, the Raikoke volcanic eruption (Kuril Islands, Russia), in June 2019 (Kloss et al., 2021; Vaughan et al., 2021; Cameron et al., 2021; Gorkavyi et al., 2021), increased the background aerosol in the upper troposphere and lower stratosphere (UTLS). For this reason, by the start of MOSAiC campaign (Multidisciplinary drifting Observatory for the Study of Arctic Climate; Shupe et al., 2022) in autumn 2019, Ohneiser et al. (2021) expected to find a residual volcanic layer with an AOD of 0.005-0.010 at 500 nm. However, they found a persistent layer of 10 km depth in the UTLS with an AOD of 0.1 and a clear wildfire smoke signature. Their analysis indicated that the conditions during the strong wildfires in Siberia at the end of July and in August were favorable for the self-lifting of the smoke, which was afterwards transported eastward until it reached Europe. Also lidar observations in Leipzig (Germany) corroborated that the Siberian wildfires reached the stratosphere. These findings led Pulimeno et al. (2024) to analyze in-situ surface measurements in Ny-Ålesund (Svalbard) during summer and

https://doi.org/10.5194/egusphere-2025-3423
Preprint. Discussion started: 15 September 2025

autumn 2019, but this surface analysis did not exhibit any notable peak events. In addition, the chemical analysis revealed only a 2 % contribution of biomass burning to the total concentration averaged during the whole investigated period.

With this framework, the main goal of this paper is to identify and characterize the aerosol events that led to the exceptional situation observed in Ny-Ålesund during the summer and autumn of 2019 and to evaluate the radiative impact observed at Ny-Ålesund during this period. For this, all available aerosol-related information for the Arctic region of Svalbard during the summer of 2019 has been compiled in order to conduct a multi-instrumental analysis of the surface and profile aerosol data for the summer of 2019.

This paper is organized as follows: Section 2 provides a brief description of the measurement sites, instrumentation and data used. Section 3 presents the main results: an overview of the temporal evolution of the measurements for different instruments; identification of the periods with aerosol events in the column and surface; analysis of the aerosol properties during these events; determination of the aerosol source using the dispersion model; quantification of the radiative impact. The main conclusions and outlooks are summarized in Section 4.

2 Sites, instrumentation and data

2.1 Sites

Svalbard is an archipelago in the European Arctic Ocean, right to the east of Greenland, from which it is separated by the Fram strait. The northernmost population in Svalbard is Ny-Ålesund, situated on the west coast of the biggest island of the archipelago, Spitsbergen (see Figure 1). Ny-Ålesund is located in the shore of Kongsfjord, which ends in easterly direction at a large ice field and is surrounded by glaciers and mountains of about 700 m height. Around Ny-Ålesund, several measurement sites have been established. Within the village, two major sites are located: the joint German-French Arctic station AWIPEV (Alfred Wegener Institute for Polar and Marine Research and the Polar Institute Paul-Émile Victor) and the Ny-Ålesund Research Station Sverdrup, from the Norwegian Polar Institute (NPI). The Zeppelin Observatory (ZEP) is located on top of the Zeppelin Mountain, about 2 km south to the village. ZEP is run by the NPI and the Norwegian Institute for Air Research (NILU). The Gruvebadet Atmospheric Laboratory (GAL), where the Italian CNR (Consiglio Nazionale delle Ricerche) operates its instrumentation, is located halfway between ZEP and Ny-Ålesund. In the southern part of Spitsbergen, at a fjord with which it shares name, the Institute of Geophysics Polish Academy of Sciences operates the Polish Polar Station, Hornsund. The location of these stations can be seen in Figure 1.

In addition to the ground stations, data recorded onboard the research vessel R/V OCEANIA, which was travelling through the Fram strait during the period of study, has been used. The aerosol measurements from these observatories for the 2002-2020 period from Hansen et al. (2022) built the basis data for this study. This data has been complemented with additional measurements recorded in the same observatories and information from CALIPSO satellite (Cloud-Aerosol Lidar and Infrared Pathfinder Satellite Observation). A summary of the sites, instruments and data products used in the study can be seen in Table 1. A brief description of the instrumentation, data products and the FLEXPART model setup used for the analysis is given in the following section.

https://doi.org/10.5194/egusphere-2025-3423
Preprint. Discussion started: 15 September 2025

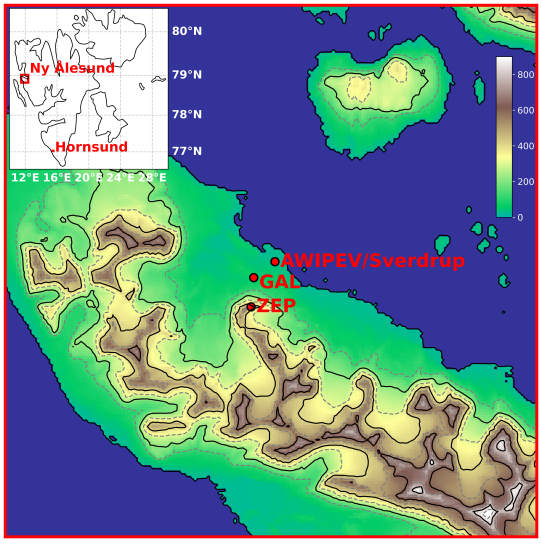

Figure 1. Topographic map of the vicinity of Ny-Ålesund and its location on Svalbard. Map created using the dataset by Moholdt et al. (2019).

2.2 Instrumentation and data

2.2.1 Sun-photometers

Sun-photometers measure direct sun spectral irradiance, which is used to derive the AOD at different wavelengths. AOD is an indicator of the amount of aerosol in the atmospheric column. In addition, the Ångström exponent (AE) can be calculated from the spectral dependence of the AOD for the range of wavelengths available. AE is related to the aerosol particle size.

Different models of sun-photometers are distributed around Svalbard. A precision filter radiometer (PFR; Kazadzis et al., 2018; Kouremeti et al., 2022) and a sun photometer 1 automatic (SP1A; Herber et al., 2002; Mazzola et al., 2012; Graßl and Ritter, 2019) are located at the Sverdrup and the Zeppelin Observatory respectively. In Hornsund, there is a CE318-T (Cimel Electronique) belonging to the Aerosol Robotic Network (AERONET; Holben et al., 1998). CE318-T instruments can also measure sky radiances at various wavelengths, which are then used together with simultaneous AOD measurements to retrieve microphysical and optical aerosol properties using an inversion algorithm (Sinyuk et al., 2020). Finally, a Microtops II manual photometer onboard the research vessel Oceania was used to complement the fixed location measurements with AODs from different locations around the Svalbard Archipelago. This instrument is part of the maritime aerosol network from AERONET (Smirnov et al., 2009), and is used to provide ship-borne AOD measurements. The Micorotops II sun photometer technical parameters as well as calibration techniques can be consulted in Morys et al. (2001) and Markowicz et al. (2012). During the 2019 study, each measurement slot lasted for about 1 minute. In order to reduce potential human errors (e.g. sun pointing error),

https://doi.org/10.5194/egusphere-2025-3423
Preprint. Discussion started: 15 September 2025

Table 1. Summary of sites, instrumentation and data products.

Site	Coordinates	Instruments	Product
AWIPEV	78.92°N, 11.92°E	SP1A	AOD 500 nm
	7 m a.s.l.	KARL	Backscatter profiles at 355, 532 and 1064 nm, polarization at 532 nm
		CHP1 Pyrheliometer	DNI
		CMP22 Pyranometer	DIF
Sverdrup	78.92°N, 11.93°E	PFR	AOD 500 nm
	10 m a.s.l.		
GAL	78.92°N, 11.89°E	PSAP	Aerosol absorption coefficient
	20 m a.s.l.	Nephelometer	Aerosol scattering coefficient
		SMPS, APS	Aerosol particle number size distribution
ZEP	78.91°N, 11.89°E	SP1A	AOD 500 nm
	474 m a.s.l.	MAAP	Aerosol absorption coefficient
		Nephelometer	Aerosol scattering coefficient
		DMPS	Aerosol particle number size distribution
Hornsund	77.00°N, 15.54°E	CE318-T	AOD 500 nm, AE 440-870, volume size distribution and single scattering albedo at 440, 675, 870 and 1020 nm
	12.5 m a.s.l.		
R/V	67°N-85°N,	Microtops II	AOD at 500 nm
OCEANIA	20°W-20°E		
	0 m a.s.l.		
CALIPSO	< 50 km from Ny-Ålesund	CALIOP	Aerosol extinction profiles at 532 nm, tropospheric and stratospheric AOD at 532 nm, tropopause altitude

5 scan slots with each measurement and the scan with the lowest standard deviation was further regarded for the processing analyses. For this study only data recorded when the vessel was 50 km distance or less from Ny-Ålesund have been used.

The sun-photometer dataset used in this study from Hansen et al. (2022) includes the AOD at several wavelengths (depending on the instrument) and the AE derived in the range 380-870 nm. The comparability of the AOD from the different sun-photometers was already assessed within the mentioned projects. For this analysis, hourly and instantaneous values of AOD at 500 nm and AE in the 380 and 870 nm range have been used. In addition, particle volume size distribution (PVSD) and single scattering albedo (SSA) have been directly obtained from the AERONET website (https://aeronet.gsfc.nasa.gov/, last accessed September 5, 2025) as the AERONET inversion algorithm level 1.5 products (version 3). These retrieved properties have been filtered by the residual obtained by the inversion algorithm; inversions with residuals bigger than 10 % have been rejected. For the period of study the PVSD and SSA are only available at Hornsund.

https://doi.org/10.5194/egusphere-2025-3423
Preprint. Discussion started: 15 September 2025

2.2.2 In-situ observations

In-situ aerosol optical and microphysical properties are measured continuously at ZEP and GAL. At these two sites the aerosol absorption coefficient (β_{abs}) and the aerosol scattering coefficient (β_{sca}) both at 530 nm, and the particle number size distribution (PNSD) between 10 – 700 nm are recorded. In addition, the single scattering albedo at the same wavelength (SSA_{530}) can be calculated as the ratio between the scattering coefficient and the scattering coefficient plus the absorption coefficient.

At ZEP, β_{abs} was originally measured at 637 nm using a multi-angle absorption photometer (MAAP, Thermo Fisher Scientific Inc., Germany, model 5012), and after converted to 530 nm (assuming an AE of 1). β_{sca} was recorded using a nephelometer (Ecotech Pty Ltd., Australia, model Aurora 3000), measuring at 450 nm, 550 nm and 700 nm, and converted to 530 nm using the scattering Ångström exponent (SAE). The PNSD was measured using a twin differential mobility particle sizer (DMPS) system, consisting of two custom built Hauke-type differential mobility analysers (DMAs) each connected to a condensational particle counter (CPCs a TSI 3010 CPC and TSI 3772) used to count the size discriminated aerosol particles. All samplings were conducted using a whole-air inlet in accordance with sampling procedures laid out by the World Meteorological Organization / Global Atmosphere Watch (WMO/GAW) guidelines.

At GAL, β_{abs} was recorded with a Particle Soot Absorption Photometer (PSAP, Radiance Research) at three wavelengths (467 nm, 530 nm, 660 nm), while β_{sca} was measured at 530 nm with a Nephelometer (Radiance Research). Raw data were corrected, averaged over 1-hour, and converted to standard temperature and pressure conditions as described by Gilardoni et al. (2023). The aerosol PNSD was continuously measured at GAL using a combination of a Scanning Mobility Particle Sizer (SMPS) model TSI 3034 and an Aerodynamic Particle Sizer (APS) model TSI 3321, both from TSI (see Rinaldi et al., 2021, and references within).

2.2.3 KARL lidar

The lidar measurements were performed by the Koldewey Aerosol Raman Lidar (KARL) at AWIPEV. This system has a Spectra 290/50 Nd:YAG laser, which emits a laser pulse at 355 nm, 532 nm and 1064 nm with 50 Hz and 200 mJ per colour vertically into the atmosphere. A telescope with 70 cm diameter collects backscattered photons with a field of view of about 2 mrad. Data recording is done via Hamamatsu photomultipliers and Licel transient recorders with a raw resolution of 7.5 m and 82 s. Both, analogue and photo counting signals, are recorded. Full overlap is reached at about 700 m altitude. In addition, KARL receiver can separate the backscattered signal into parallel and perpendicular components at 532 nm, which allows the calculation of the volume aerosol depolarization (δ^{aer}) as the ratio between the perpendicular and the parallel signal. This magnitude is useful to distinguish between spherical and non-spherical particles. A more detailed description of KARL can be consulted in Hoffmann (2011).

The aerosol backscatter profiles at the three available wavelengths have been used in the study. To achieve a better signal-to-noise ratio, several profiles were averaged to a 60 m and 600 s resolution for this study.

https://doi.org/10.5194/egusphere-2025-3423
Preprint. Discussion started: 15 September 2025

The backscatter profiles have been used to calculate the color ratio (CR), for each ((λ_1, λ_2)) combination of the three laser wavelengths as Equation 1:

$$CR(\lambda_1, \lambda_2) = \frac{\beta^{aer}(\lambda_1)}{\beta^{aer}(\lambda_2)} \qquad \text{with } \lambda_1 < \lambda_2 \tag{1}$$

To adjust for measurement uncertainties, an uncertainty of ± 5 % of the CR has been considered. The CR can be also be theoretically estimated using the Mie calculator from Library for Radiative Transfer – libRadtran (Mayer and Kylling, 2005; Emde et al., 2016). For this calculus we have assumed a log-normal particle size distribution with a width of $\sigma = 1.1$ and a refractive index of $m = 1.5 + 0.05i$; which is a typical refractive index for Arctic aerosol (Böckmann et al., 2024).
The best fit between the theoretical and observed color ratios for each combination of the available wavelengths 355, 532 and 1064 nm has been used to estimate the height-dependent effective radius of the aerosol. This way, vertical profiles of the aerosol effective radius have also been obtained.

2.2.4 Surface radiation

The set-up of surface radiation observations established at AWIPEV includes direct normal irradiance (DNI) by a CHP1 pyrheliometer, diffuse (DIF), global and reflected shortwave horizontal solar irradiance by CMP22 pyranometers, as well as up and downward longwave radiation by CGR4 and Eppley PIR pyrgeometers. All instruments follow the World Radiometric Reference (WRR) standards for solar radiation data and the World Infrared Standard group (WISG) guidelines for longwave radiation. Additionally, the data contributes to Reference Upper-Air Network (GRUAN). The surface radiation measurement setup, data retrieval, and quality control follow Baseline Surface Radiation Network (BSRN) standards. More information is given by König-Langlo et al. (2013) and Maturilli et al. (2015), among others. All measurements were performed automatically with a 1-min resolution and can be found in Maturilli (2020) (https://doi.org/10.1594/PANGAEA.914927). These data are available since 2006.

The hourly anomaly (Δ_{DNI}) for the hourly DNI values has been calculated with respect to a reference value (DNI_{ref}), as shown in Equation 2:

$$\Delta_{DNI} = DNI - DNI_{ref} \tag{2}$$

The DNI_{ref} values have been calculated for each month and each hour as the mean of all DNI hourly values recorded at that specific hour during that month from the 2006 to 2020 reference period. As a result, 24 reference values are obtained for each month. This approach is used because, due to the high frequency of cloudy conditions in the region, the amount of available data to construct a reliable reference is limited.

In addition, the diffuse ratio (DifR; see Long et al., 1995) has been calculated following Equation 3:

$$\mathrm{DifR} = \frac{\mathrm{DIF}}{\mathrm{DIF} + \mathrm{DNI} \cdot \cos(\mathrm{SZA})} \tag{3}$$

https://doi.org/10.5194/egusphere-2025-3423
Preprint. Discussion started: 15 September 2025

This ratio can take values from zero to the unit, being small values related to cloud-free cases. Only data showing an hourly DifR < 0.3 have been used, trying to reject the influence of clouds on the results.

2.2.5 CALIOP

CALIOP (Cloud-Aerosol LIdar with Orthogonal Polarization) is the main instrument onboard CALIPSO satellite. CALIPSO was launched on April 2006 (Winker et al., 2009) and after 17 years of operation, it ended its mission on 1 August 2023.

CALIOP consists of a two-wavelength lidar that uses a Nd:YAG laser to emit pulses at 1064 and 532 nm simultaneously. The laser pulse repetition frequency is 20.16 Hz, which allows a horizontal resolution of 335 m at the ground. The outgoing 532 nm pulses are linearly polarized. A polarization beam splitter separates the components of the 532 nm backscatter signal polarized parallel and perpendicular to the plane of the outgoing beam, which are collected by two detectors. The instrument operates continuously, providing observations during both day and night.

In this work it has been utilized the level 2 (L2) profile data products (LID_L2_05kmAPro-Standard-V4-51) for aerosol extinction at 532 nm, which is given at a spatial resolution of 60 m vertically and horizontal averaging length of 5 km along the satellite track. The L2 layer data product (LID_L2_05kmALay-Standard-V4-51) includes the tropospheric and stratospheric AOD at 532 nm, as well as the L2 vertical feature mask (LID_L2_VFM-Standard-V4-51) for aerosol and cloud classifications. The tropopause altitude is also included in the CALIPSO dataset.

CALIPSO data have been downloaded from the ICARE Data and Services Center (http://www.icare.univ-lille1.fr/, last access: 23 August 2023). For this analysis, data within 50 km distance from Ny-Ålesund have been extracted, and the closest extinction profile has been utilized (see supplementary Figure S1).

2.2.6 Atmospheric dispersion modelling/FLEXPART

To investigate the possible origin of BC (black carbon) aerosol air-masses reaching the Arctic, the Lagrangian particle dispersion model FLEXPART version 10.4 has been used (Pisso et al., 2019). The model has been driven by hourly reanalysis meteorological fields (ERA5) from the European Centre for Medium-Range Weather Forecasts (ECMWF) with 137 vertical levels and a horizontal resolution of $0.5° \times 0.5°$ (Hersbach et al., 2020). Computational particles have been released in FLEXPART at various heights (0 - 100, 100 - 500, 500 - 4000, 4000 - 6000, 6000 - 10000 m) from the receptor (considered the Zeppelin Observatory) and tracked backward in time in FLEXPART's "retroplume" mode. Simulations have been run 30 days back in time, that is a sufficient time to include most BC sources arriving at the station, given a typical BC lifetime of 1 week (Bond et al., 2013).

Gravitational sedimentation for spherical particles is included and differs between trajectory models due to its ability to simulate dry and wet deposition of aerosols (Grythe et al., 2017), turbulence (Cassiani et al., 2015), unresolved mesoscale motions (Stohl et al., 2005), and convection (Forster et al., 2007). In the simulations of this work it has been assumed that BC has a density of $1500\ \mathrm{kg\,m^{-3}}$ and follows a logarithmic size distribution with an aerodynamic mean diameter of $0.25\ \mu$m and a logarithmic standard deviation of 0.3 (Long et al., 2013).

https://doi.org/10.5194/egusphere-2025-3423
Preprint. Discussion started: 15 September 2025

Anthropogenic emissions have been adopted from the latest version (v6b) of the ECLIPSE (Evaluating the CLimate and Air Quality ImPacts of ShortlivEd Pollutants) emission inventory, an upgraded version of the previous version (Klimont et al., 2017). This inventory includes industrial combustion emissions, emissions from the energy production sector, residential and commercial emissions, emissions from waste treatment and disposal sector, transportation, shipping activities and gas flaring emissions. Biomass burning emissions have been adopted from the Copernicus Global Fire Assimilated System (CAMS GFAS) (Kaiser et al., 2012) because this product provides an estimation of the injection altitude of the fire emissions.

FLEXPART simulations have been performed every 3 hours during the studied period. The FLEXPART output consists of a footprint emission sensitivity, which results in a modeled concentration at the receptor (Zeppelin Observatory), when coupled with gridded emissions from an emission inventory (like the ones described before). The emission sensitivity expresses the probability of any release occurring in each grid-cell to reach the receptor. The modelled concentrations can be displayed as a function of the time elapsed since the emission has occurred (i.e., "age"), which can be shown as an "age spectrum". Detailed source contribution maps have been calculated, showing which regions contributed to the simulated concentration.

The source contributions to receptor BC have been derived by combining each gridded emission sector (e.g. gas flaring, transportation, waste management, etc) from an emission inventory with the footprint emission sensitivity. Calculations for anthropogenic sources and open biomass burning have been performed separately. This has enabled the identification of the exact origin of BC and allowed for quantification of its source contribution.

3 Results

3.1 General overview

The data obtained from the various instruments described in the previous section have been analyzed to characterize the aerosol reaching Svalbard in summer 2019. First, an analysis of the columnar aerosol load has been conducted using sun-photometry. Next, data from in-situ observatories have been used to analyze the aerosols reaching the surface. Finally, active remote sensing instrumentation has been used to identify the altitude at which the aerosol intrusion is occurring.

3.1.1 Columnar aerosol

Figure 2 shows the hourly AOD values at 500 nm (AOD_{500}) recorded in and around Svalbard from June to September 2019. The mean daily AOD_{500} values calculated considering all the available period (2002-2020) are included as reference (see dashed line in Figure 2). It can be seen that most of the summer of 2019 (considered from June to September for this study, if nothing else is specified) presented consistently higher values of AOD with respect past and following years (2002 to 2020 period). AOD_{500} in 2019 was similar to the reference values during June, but since 6 July, when an unprecedented increase in AOD occurred, it remained high for the rest of the summer. The median AOD_{500} from July to September for the 2002-2020 reference period is 0.048, but this value is 0.162 when it is calculated only with 2019 data; it means that AOD_{500} in this period was more than three times higher than during the reference. Regarding the AE, which is related to the size of the aerosol, it

https://doi.org/10.5194/egusphere-2025-3423
Preprint. Discussion started: 15 September 2025

did not show a significant difference with respect to the reference period as can be observed in the supplementary Figure S2. The days on which the AOD_{500} values were higher than the summer average plus three times the standard deviation have been identified as days when an aerosol intrusion was occurring in Svalbard. This way, three different aerosol events have been identified during the summer of 2019 in the following periods: 6 to 10 July, 25 to 28 July and 6 to 17 August, which have been named C1, C2 and C3 respectively because they are observed in the atmospheric column (C). During these three events the mean AOD_{500} values were 0.28, 0.19 and 0.23 respectively. Moreover, the periods between C1 and C2, and between C2 and C3 presented mean AOD_{500} values of 0.15 and 0.17 respectively; this mean value was 0.15 from the end of event C3 (17 August) to the end of August. Finally, during September the mean AOD_{500} was 0.11.

The columnar PVSD and SSA values retrieved for the analyzed period are shown in Figure 3, highlightening those corresponding to the identified events. Table 2 collects the mean AOD and mean parameters of the PVSD, observed during the periods identified with aerosol event, and also in the adjacent periods during summer 2019. Figure 3a-d shows a high aerosol concentration in fine mode (Accumulation mode) during July and August; this also happens for September, when no aerosol events have been identified. Aitken mode and coarse mode particles are almost absent; the highest variability in PVSD during this summer is observed in the Accumulation mode, when the peaks oscillate from 0.01 to 0.04 $\mu m^3 \mu m^{-2}$ in all the period.

In July, the mean effective radius of the fine mode ($< R_{eff}F >$) was 0.145 μm the days with no aerosol event, and 0.156 μm and 0.155 μm in events C1 and C2, respectively. However, while C1 showed a slim fine mode distribution with one maxima, C2 generally a main maxima at radius about 0.1 μm and a second maxima at about 0.3 μm. This might indicate the presence of particles of different origin during C2.

In August, the fine mode distribution was wider and with a gaussian shape, presenting in general lower concentrations at each radius. Event C3 presented the highest $< R_{eff}F >$ (0.182 μm) of the three identified events. This might either point to different aerosol source or be an aging effect, such that the mean time between the aerosol emission and arrival over Spitsbergen might be longer in August compared to July. This longer radii made AE values lower in event C3 (see Figure S2) than in the other events even when all were dominated by fine particles (González et al., 2020). Nevertheless, days not identified as aerosol intrusion showed a distribution similar to the ones observed during event C2, with a mean $< R_{eff}F >$ of 0.156 μm.

In September only two inversions are available (on the 5th). These presented a $< R_{eff}F >$ of 0.142 μm and, again, a similar shape, but with a lower concentration at each radius than the ones observed in event C2 (July). However, the coarse mode seems slightly enhanced and these particles, larger than 2 μm, should sediment down quickly. As similar observations are made throughout July, August and September, this might indicate a steady supply of new aerosol (because of the life-time of this coarse particles). Alternatively, due to the low concentration of the coarse mode, it could just indicate the presence of a steady stratospheric aerosol starting from event C2, which was combined with new aerosol with the arrival of new aerosol events. Therefore it can be hypothesized that we are facing a combination of different aerosol sources.

The SSA, shown in Figure 3e-h, presents values close to 1 for all wavelengths, indicating a low aerosol absorption even during the aerosol events. Only a few background cases showed values lower below 0.96 in the infrared, but these cases do not show up for the identified events, indicating less variability. The high SSA and no spectral dependency during the events could be caused by the presence of BB aged after long transport (Zielinski et al., 2020) or might have been emitted under low

https://doi.org/10.5194/egusphere-2025-3423
Preprint. Discussion started: 15 September 2025

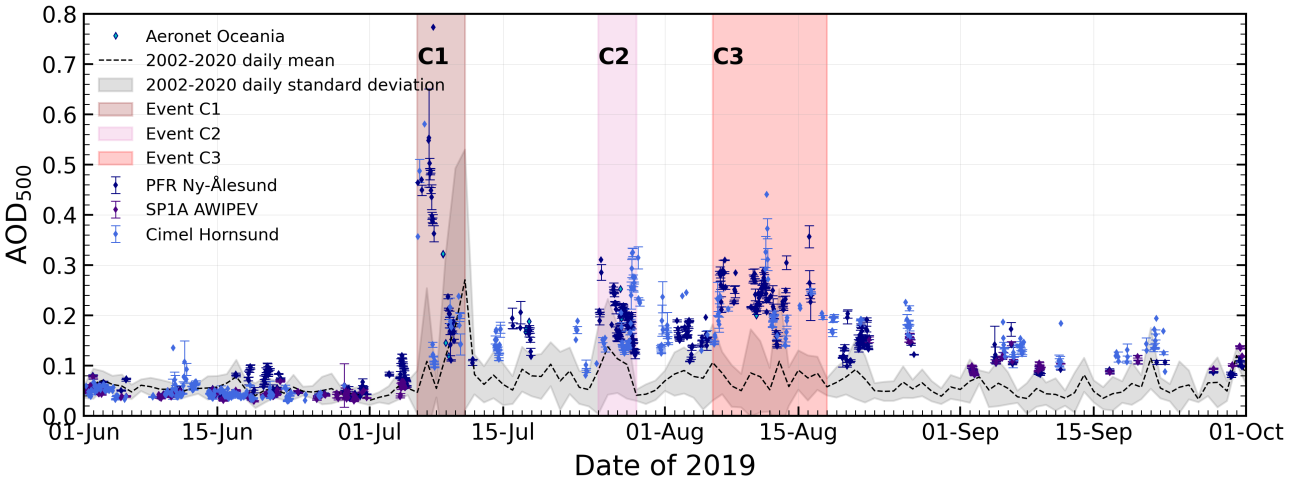

Figure 2. Aerosol Optical Depth (AOD) temporal evolution (hourly means with standard deviation) in and around Svalbard in the summer of 2019 (June to September), with data from Ny-Ålesund, Hornsund and Oceania (in the Fram Strait). Long-term daily means and the corresponding standard deviation of all available ground-based measurements are represented by the black dashed line and grey shaded area respectively. The time periods highlighted in red shaded area correspond to the three events identified as aerosol events in the column: 6-10 July (C1), 25-28 July (C2) and 6-17 August (C3). The scatter points with errors bar represent hourly mean values and their associated standard deviation. The black dashed line represents the mean daily values of AOD at 500 nm calculated with all the available measurements on the reference period, i.e. from 2002 to 2020; the grey shaded area represents the corresponding standard deviation.

Table 2. Mean values of the aerosol optical depth (AOD) and the parameters of the PVSD: effective radius (R_{eff}), standard deviation (σ), and volume concentrations (VC), for fine (F) and coarse (C) modes, and the total volume concentration (VCT), during the different periods identified with aerosol event, and adjacent periods during summer 2019 (June to September).

	AOD	$R_{eff}F$ [μm]	σF [μm]	VCF [$\mu m^3 \mu m^{-2}$]	$R_{eff}C$ [μm]	σC [μm]	VCC [$\mu m^3 \mu m^{-2}$]	VCT [$\mu m^3 \mu m^{-2}$]
June	0.05	0.149	0.448	0.005	1.486	0.707	0.006	0.012
C1 (6-10 July)	0.28	0.156	0.476	0.024	1.728	0.634	0.004	0.029
11-24 July	0.15	0.145	0.537	0.037	2.328	0.663	0.002	0.039
C2 (25-28 July)	0.19	0.155	0.578	0.041	2.401	0.625	0.004	0.045
29 July - 5 August	0.17	-	-	-	-	-	-	-
C3 (6-17 August)	0.23	0.182	0.585	0.035	2.166	0.654	0.005	0.04
18-31 August	0.16	0.156	0.617	0.04	2.354	0.707	0.003	0.042
September	0.11	0.142	0.618	0.033	2.609	0.576	0.005	0.037

combustion efficiencies (Liu et al., 2014). This kind of aerosol agrees well with the predominant fine mode with an effective radius longer than usual (González et al., 2020).

https://doi.org/10.5194/egusphere-2025-3423
Preprint. Discussion started: 15 September 2025

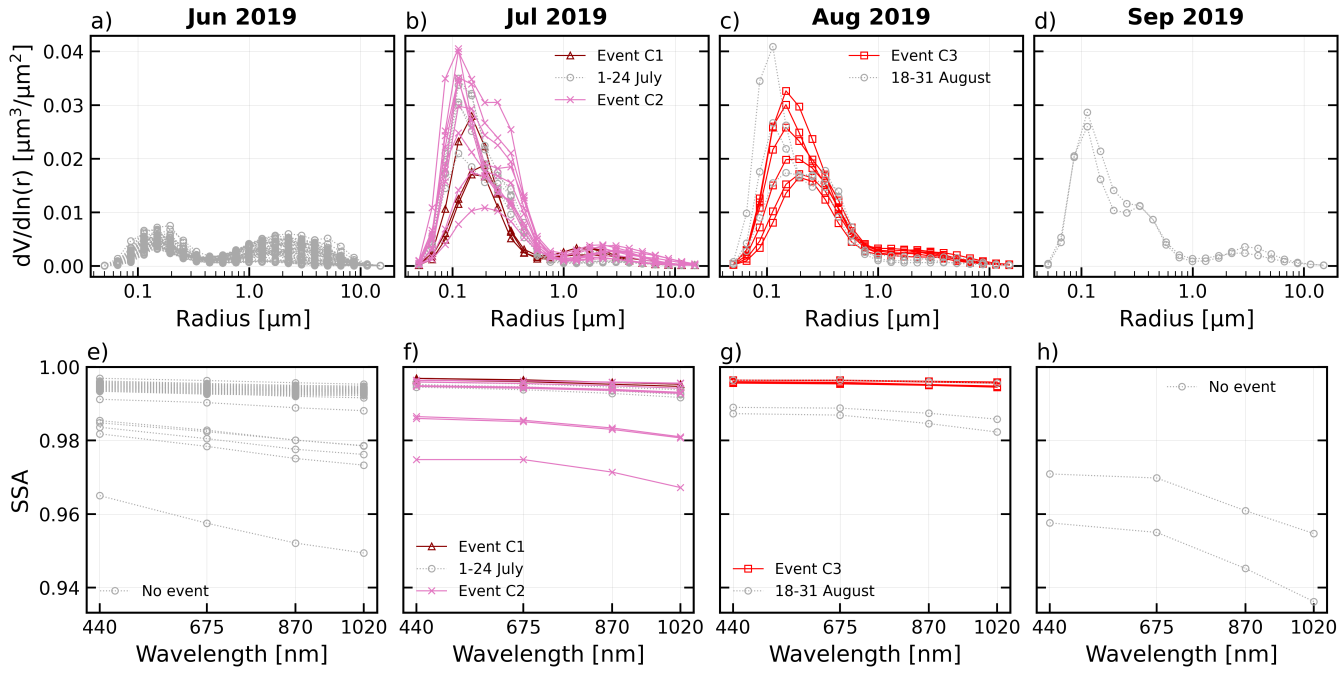

Figure 3. a-d) Columnar particle volume size distribution and e-h) Single Scattering Albedo (SSA) AERONET products available from from June to September 2019 at Hornsund. The properties corresponding to the aerosol events identified in Figure 2 have been highlighted with different markers and colors.

3.1.2 Surface aerosol

Figures 4a and b report, respectively, the time series of the aerosol absorption (β_{abs}) and the scattering (β_{sca}) coefficients at 530 nm measured in-situ at GAL and ZEP in summer 2019. During the full period, β_{abs} and β_{sca} showed the next mean values: 0.12 ± 0.16 Mm^{-1} and 1.83 ± 2.04 Mm^{-1} at GAL and 0.10 ± 0.21 Mm^{-1} and 2.43 ± 2.97 Mm^{-1} at ZEP, respectively. The average SSA_{530} was 0.92 ± 0.06 and 0.96 ± 0.06 at GAL and ZEP, respectively. The seasonal averages for the summers of 2018 and 2020 together with the ones from 2019 are included in Table 3. It shows that 2019 did not show significant differences at ground level in these type of measurements.

Table 3. Seasonal averages (and standard deviation in parenthesis) for summers (June to September) 2018, 2019 and 2020 for aerosol absorption (B_{abs}) and the scattering (B_{sca}) coefficients at 530 nm.

	GAL		ZEP	
Year	B_{abs530}	B_{sca530}	B_{abs530}	B_{sca530}
2018	0.105 (0.143)	3.696 (2.492)	0.068 (0.077)	2.787 (2.479)
2019	0.120 (0.163)	1.833 (2.045)	0.099 (0.207)	2.433 (2.966)
2020	0.161 (0.245)	2.845 (2.884)	0.115 (0.245)	1.636 (1.230)

https://doi.org/10.5194/egusphere-2025-3423
Preprint. Discussion started: 15 September 2025

The B_{abs530} at GAL and ZEP correlate with a Pearson coefficient (R) of 0.71. A lower correlation is observed for B_{sca530}, with an R of 0.34, although increasing and decreasing trends have been generally observed at the same time at the two sites. This low R points towards a more local origin for scattering aerosol, so that while the absorption is predominantly due to long-range transport, the scattering in summer has a more important marine source and if the wind direction at both sites does not agree the stations perceive this local source differently. However, whenever a strong event comes, the scattering increases in both sites. Therefore, it is difficult to use only one station for comparison with climate models.

Aerosol events at the surface, associated with relatively high aerosol loading at the ground, have been identified when both B_{abs530} and B_{sca530} exceeded, at least in one station, the average values recorded over three summers (2018-2020, from June to September), plus three times the standard deviation (horizontal lines in Figure 4). This way, three events of high aerosol load on the surface (S) have been identified on 5 to 9 July, 30 August, and 12 September. The first event (5 to 9 July) overlaps in time with event C1, therefore we will refer to it as CS1 instead of C1 from now on. The last two events have been named events S1 and S2 respectively. No data from remote sensing observations were available during these two events due to cloudy conditions.

The increase in absorption coefficient observed during the three surface events points to the impact of air masses affected by combustion emissions. The SSA_{530} observed during events S1 and S2 were 0.89 ± 0.04 and 0.92 ± 0.05, respectively, reaching values as low as 0.81 (event S1) and 0.76 (event S2). For event CS1 the mean SSA_{530} was 0.95 ± 0.01 with lowest values equal to 0.92. The slightly lower SSA_{530} values observed during the events S1 and S2 might indicate that the aerosol particles emitted by combustion traveled a shorter distance before reaching Svalbard compared to event CS1, although the differences are within the standard deviations.

Figure 5 reports the averaged particle number size distribution during the surface events and for all available measurements in the summer of 2019. The PNSD values observed at the two sites align with the multi-year average distributions reported by Dall'Osto et al. (2019) for the summer months. With respect GAL observations, the seasonal average of PNSD exhibits a bimodal pattern, with peaks occurring at approximately 30 nm (Aitken mode) and 140 nm (Accumulation mode). The Aitken mode predominates over the Accumulation mode, primarily due to new particle formation events that increase the number of ultrafine particles (Dall'Osto et al., 2019; Tunved et al., 2013b). Additionally, wet scavenging removes effectively Accumulation mode particles in summer both in the Arctic and during their transport to the Arctic (Dall'Osto et al., 2019; Gilardoni et al., 2019). The surface events were still characterized by a bimodal distribution, but in these cases the particle number of the Accumulation mode was comparable or higher than the Aitken mode population, indicating that the site was reached by more aged aerosol populations. The increase in Accumulation mode particles agrees with the rise in scattering coefficients during the three events compared to the average.

3.1.3 Aerosol vertically-resolved properties

A time series with the CALIOP aerosol extinction profiles (at 532 nm) available in summer 2019 is shown in Figure 6. The tropospheric and stratospheric AODs retrieved from CALIPSO for each profile are also included in the upper panel. For event CS1 a strong extinction is observed between 3 and 5 km a.g.l. Starting from 15 July a stratospheric aerosol layer at about 12 km

https://doi.org/10.5194/egusphere-2025-3423
Preprint. Discussion started: 15 September 2025

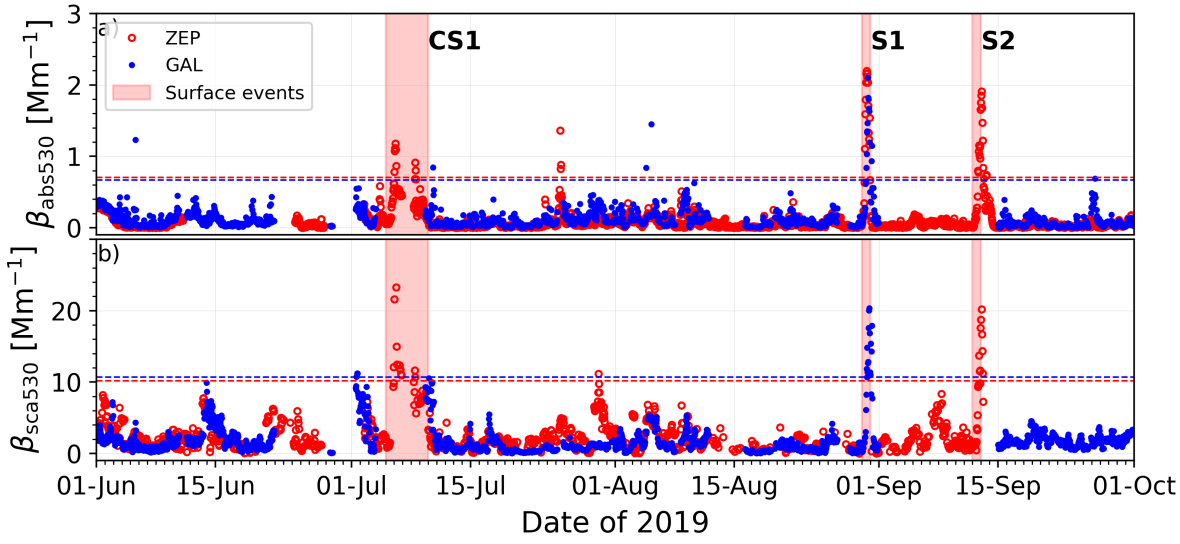

Figure 4. Time series of a) aerosol absorption coefficient (B_{abs}) and b) scattering coefficient (B_{sca}) at 530 nm at Gruvebadet (GAL), in blue, and Zeppelin (ZEP), in red. The horizontal lines correspond to the average of the logarithm of scattering and absorption coefficients over three summers (2018-2020, from June to September) plus three times the standard deviation (in blue for GAL and in red for ZEP) used to identify aerosol events. The time periods with red shaded areas correspond to the three events identified as high aerosol load in the surface: 5 to 9 July (CS1), 30 August (S1), and 12 September (S2)

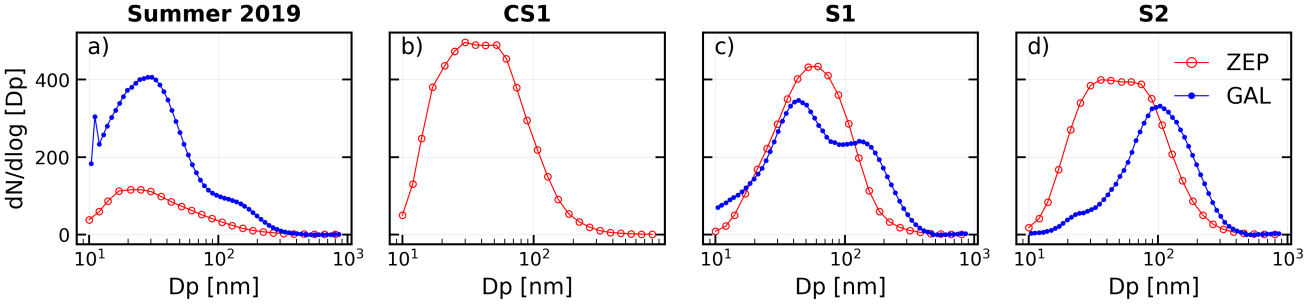

Figure 5. Average particle number size distribution (PNSD) at Gruvebadet (GAL), in blue, and Zeppelin (ZEP), in red, during the summer of 2019 (June to September) (a) and events CS1 (b), S1 (c) and S2 (d). For CS1 the are only data from ZEP.

a.g.l. is observed, with the corresponding increase in the stratospheric AOD. An aerosol layer between 10 and 15 km a.g.l. is also observed in the following extinction profiles, with variable intensity. During C2 and C3, no clear signature of aerosols is observed in the troposphere, maybe related to the presence of tropospheric clouds, which would mask the aerosol when

https://doi.org/10.5194/egusphere-2025-3423
Preprint. Discussion started: 15 September 2025

observing from a satellite.

Unfortunately, KARL measurements are only available for four days in the summer of 2019; these are shown in Figure 7. Only one of these days corresponds to a day identified with aerosol event, 11 August (C3). During this day, a very high backscatter coefficient at 532 nm up to about 1 $\mathrm{Mm}^{-1}\mathrm{sr}^{-1}$ is observed in the entire troposphere, as well as in the stratosphere up to nearly 16 km a.g.l.. Particularly, the temporally stable layer just around the tropopause observed with KARL correlates very well in altitude with the increased backscatter profile measured by CALIOP at around 10 km a.g.l. in the same date. On the other available days with KARL observations, the lower stratosphere (up to around 16 km a.g.l.) had in all cases several thin aerosol layers with a comparably strong backscatter coefficient. The troposphere showed a high and constant backscatter coefficient through August, but it slowly decreased on 17 September to about 30 % of the values from 2 August.

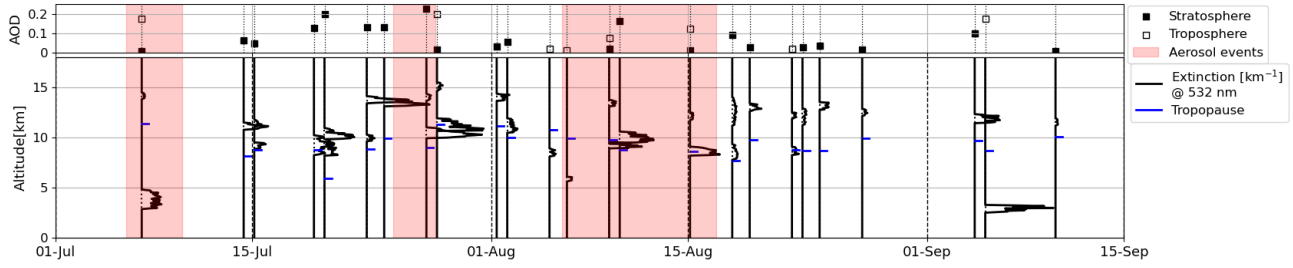

Figure 6. Time series of the extinction profiles at 532 nm measured by CALIOP in the summer of 2019. The blue lines indicate the tropopause. The tropospheric and stratospheric AOD at 532 corresponding to each profile is included in the upper panel. The red shaded areas indicate the days on which the columnar events were identified (CS1, C2 and C3).

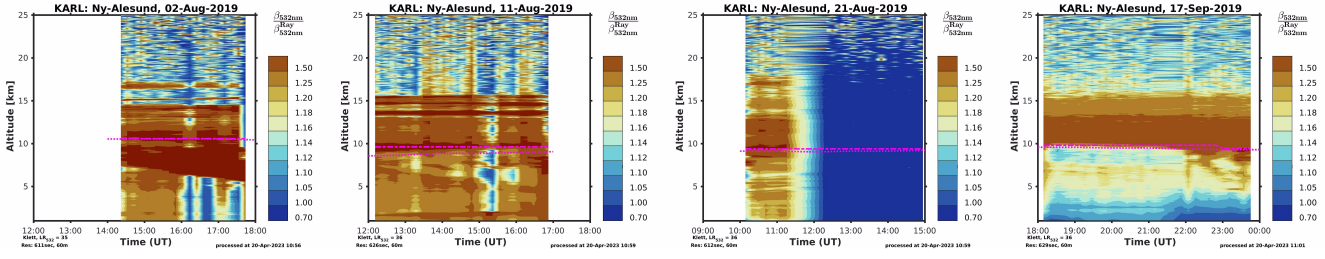

Figure 7. Backscattered signal profiles at 532 nm from KARL for 2, 11 and 21 August and 17 September. The pink lines indicate the altitude of the tropopause, which is derived from temperature profiles from radio-soundings at Ny-Ålesund as the altitude at which the lapse rate is smaller than 2 Km^{-1}.

Since the aerosol layers were temporally quite constant on each day, a daily average of the backscatter profile has been calculated to estimate the height-dependent effective radius of the aerosol for each day, as described in Section 2.2.3. The calculated effective radii for the four observation days is shown in Figure 8 with a height resolution of 60 m. Due to the

https://doi.org/10.5194/egusphere-2025-3423
Preprint. Discussion started: 15 September 2025

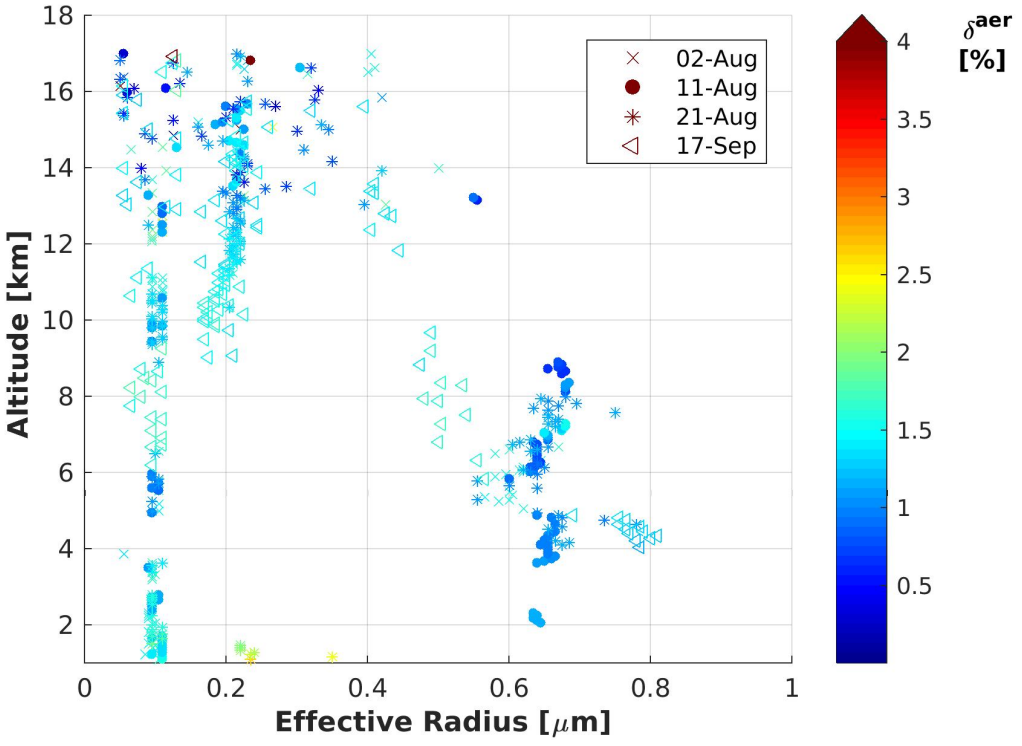

Figure 8. Averaged height-dependent estimation of the effective radius determined for during Lidar observations until 18 km altitude in correlation with the aerosol depolarization, δ^{aer}, for all four observation days with KARL.

incomplete lidar overlap, the plot starts at 1 km altitude. This figure shows that for all days and the entire troposphere the background aerosol had radii values at around 0.1 μm, while the pronounced layers reveal coarser aerosols with radii from 0.5 μm to 0.8 μm. Furthermore, it can be seen that the effective radius for August was very similar, while on 17 September, between 7 and 9 km a.g.l., the effective radius was about 0.2 μm smaller. This suggests that the largest particles were removed from this layer, possibly due to sedimentation. Depolarization measurements at 532 nm ($\delta^{aer} < 3$ %) were lower than 3 % for the four available days. These low values are typical for a spherical shape. Hence, we conclude that the large particles in the troposphere were likely droplets. Hygroscopically grown particles act directly as Cloud Condensation Nuclei (CCNs) and grow in the water phase, but do not serve as Ice Nucleating Particles (INPs). This can be seen in the low depolarization throughout the entire studied atmosphere. Furthermore, this process happened quickly, because otherwise the gap in effective radius in the troposphere between 0.2 μm to 0.5 μm would not exist. At an altitude of about 1 km, a distinct aerosol type appeared on 21 August. Only on this day at that height, the depolarization reached its maximum with 2.5 %, indicating slightly less spherical shape than in the layers above.

https://doi.org/10.5194/egusphere-2025-3423
Preprint. Discussion started: 15 September 2025

In the stratosphere (from 9–10 km) a different behavior is observed. A distinct aerosol signature appeared, characterized by an effective radius of approximately 0.2 μm, although dispersed values ranging from 0.2 to 0.4 μm are also observed, particularly between 12 and 17 km a.g.l.. When comparing the results from KARL with the retrievals from photometer observations (see Section 3.1.1), the effective radii are similar. It must be noted that generally the aerosol backscatter and extinction decreases with altitude (not shown here). Hence, in Figure 8 the lower altitudes needs to be "weighted" more than high altitudes for a comparison with photometers. By comparison of Figures 3 and 8 it is obvious that the predominant mode around 0.1 μm (Accumulation) is tropospheric, while the second maximum (in Figure 3 weaker) around 0.2 μm is stratospheric. Particles > 0.5 μm seem to be less frequent in the lidar, compared to photometer. This is likely due to the selection effect that the lidar only operates during clear sky conditions. Hence, clouds are underrepresented in the lidar data. Still, some hygroscopically grown aerosol might be visible in the lidar data which we relate to the range of effective radii between 0.55 to 0.8 μm. Further, the weak coarse mode with particles > 1μm is missing in the lidar, as for this instrument we only assumed a one-modal aerosol distribution.

3.2 Origin identification

3.2.1 Columnar events CS1, C2 and C3

The footprint emission sensitivity together with the corresponding source contribution to BC and the continental contribution to BC at each model altitude for events CS1, C2 and C3 are depicted in Figure 9. These parameters have been integrated, for each event, by the temporal duration determined in the previous section. The source contribution panels in the middle column of Figure 9 indicate high concentrations of biomass burning BC during these events. Event CS1 (Figure 9, top row)is the one that presents the highest concentration, with maximum values of 140 $ng\,m^{-3}$ at 500 m a.g.l., but also a high concentration at 100 and 4000 m a.g.l. For this event the footprint emission sensitivity indicates that the BC was coming mainly from wildfires in central Siberia. The use of a continental mask indicated that the contribution of BC from fires in Russian territory was more than 95 % at heights between 0 and 4 km.a.g.l. (Figure 9).

Similarly, the highest BC concentrations during event C2 (Figure 9, middle row) were obtained at 4000 m a.g.l. However, modeled concentrations reached a maximum of only 40 $ng\,m^{-3}$. The source contribution to column BC shows that BC had two branches of origin, one from Siberia and another from North America. Wildfires contributed over 70 % of the BC mass arriving at the station at altitudes up to 4 km, and above 97 % of the mass was coming from Russia.

Finally, for event C3 (Figure 9, bottom row), the modeled BC concentrations at different heights reached a maximum at 4000 and 500 m a.g.l., with almost 70 and 60 $ng\,m^{-3}$ respectively. While the footprint emission sensitivity shows impact from Canada, the majority of the air masses arriving at the Zeppelin Observatory originated from central and western Siberia at 4000 m a.g.l. North American fires dominated only at lower altitudes of up to 500 m a.g.l. This last event was the second most intense observed during this summer, showing a good correlation with the AOD values observed in Section 3.1.1. In addition,

https://doi.org/10.5194/egusphere-2025-3423
Preprint. Discussion started: 15 September 2025

both C2 and C3 showed a important contribution from North America. This agrees well with the hypothesis of the long range transport considered after observing a wide and uniform aerosol side distribution in Section 3.1.1 in these events, specially for C3.

3.2.2 Intermediate periods with high AOD: from 14 July

During the periods between the aerosol events described above, relatively high AOD values have been also observed (AOD at 500 nm around 0.15-0.20 in July and August, dropping to 0.10-0.15 in September), which corresponded to fine aerosol with low absorption (see Section 3.1.1). Modelling BC levels calculated using the described emissions inventory did not show a clear source of the aerosol. At around that period, an unexpected series of blasts from a remote volcano in the Kuril Islands (Raikoke volcano) sent ash and volcanic gases streaming high over the North Pacific Ocean (Gorkavyi et al., 2021). The dormant period ended around 18:00 UTC on 21 June 2019, when a vast plume of ash and volcanic gases shot up from its 700-meter-wide crater. Several satellites observed as a thick plume rose and then streamed eastwards (McKee et al., 2021; Kloss et al., 2021). Kloss et al. (2021) observed that afterwards, the plume separated into an ash-dominated component in the south and a SO_2-dominated component in the north. While the ash plume rapidly diluted and could not be further followed, the SO_2 plume persisted. On 23–27 June 2019 parts of the dispersed SO_2 cloud, which were observed with the Microwave Limb Sounder (MLS) satellite data, presented heights between 11 and 18 km, with a peak concentration at 14 km (Gorkavyi et al., 2021).

Therefore, we further simulated the Raikoke eruption using a new inventory for the volcanic SO_2 emissions (Osborne et al., 2022). The vertical cross-sections of the modeled volcanic SO_2 arriving at Ny-Ålesund is illustrated in Figure 10. This figure shows that the volcanic aerosol reaches Ny-Ålesund specially from 14 July, when it was also observed an increase in the AOD with respect to previous AOD values. This aerosol extended in a thick layer between 7 and 15 km a.g.l. for the first two weeks since its arrival, and afterwards it was mainly present between 10 and 15 km a.g.l., which is consistent with the observations made with CALIOP and KARL in Figure 6.

Whether the aerosols observed at such altitudes were ash or soot was under strong debate. Ansmann et al. (2021) reported that the aerosol was smoke misclassified as volcanic sulfate focusing on lidar measurements in Leipzig (Germany). The reason for the misclassification was the aerosol identification algorithm that assumes non-spherical smoke particles in the stratosphere. They reported that self-lifting particles reached the tropopause within 2–7 days after emission and finally entered the lower stratosphere as aged spherical smoke particles. These spherical particles were misclassified as liquid sulfate particles. The same group hypothesized that the detected smoke during the MOSAiC (Multidisciplinary drifting Observatory for the Study of Arctic Climate) expedition in 2019-2020 originated from extraordinarily intense and long-lasting wildfires in central and eastern Siberia in July and August 2019 and may have reached the tropopause layer by self-lifting (Ohneiser et al., 2021, 2023).

On the other hand, Boone et al. (2022) concluded that the stratospheric aerosol in the second half of 2019 over the Arctic consisted of Raikoke sulfate aerosol. This study was only based on observations of stratospheric infrared absorption spectra

https://doi.org/10.5194/egusphere-2025-3423
Preprint. Discussion started: 15 September 2025

(in the framework of the satellite-based Atmospheric Chemistry Experiment mission). The authors found no indication of the presence of smoke. Gorkavyi et al. (2021) reported a high SO_2 concentration and aerosol clouds using data from the Ozone Mapping and Profiler Suite sensors on the Suomi National Polar-orbiting Partnership satellite. However, a recent comment on this publication made by Ansmann et al. (2024) states that the AOD derived from the measurements used in this analysis was four times higher than the corresponding AOD for the precited SO_2 concentration from the Raikoke volcano. In this review, it is concluded that the Arctic UTLS aerosol was likely dominated by smoke in the lower part and by sulfate aerosol in the upper part. Kloss et al. (2021) combined both observations and model simulations of the Raikoke eruption and found that a few days after the eruption, the volcanic plume was entrained in the Aleutian cyclone, and a month after, it circled the Earth (it reached Europe around 1st July). Accordingly, stratospheric AOD (sAOD) was as high as 0.045 (at 449 nm) at higher north-hemispheric latitudes, with an average value of 0.025 at longer wavelength (visible, 675 nm), while the background AOD was still enhanced in the North Hemisphere one year after the eruption. Finally, Vaughan et al. (2021) used a Raman lidar in the UK and found a thin layer at 14 km on 3rd July, with the first detection of the main aerosol cloud on 13 July, which agrees very well with our own observations in Ny-Ålesund. At that period the aerosol was confined below 16 km extending to 20 km. The authors further reported a sustained period of clearly enhanced AOD from early August, with a maximum value (at 355 nm) around 0.05 in mid-August and remaining above 0.02 until early November.

3.2.3 Surface events S1 and S2

Finally it has been investigated the origin of the surface events S1 and S2. The footprint emission sensitivity computed for the day of each event and the corresponding temporal evolution of the source and continental contributions to BC for the days of the events and days around have been plotted in Figure 11. The footprint emission for events S1 and S2 (Figure 11, left column), indicates that S1 had its source in Central Europe while, in S2, the BC is coming from Eastern Europe. This is corroborated by the continental contribution (Figure 11, right column), which shows a main contribution from Europe together with a smaller contribution from Russia, more evident in S2. Both events had an anthropogenic source, mainly due to transportation (TRA) and commercial and domestic (DOM) emissions (see Figure 11, middle column). The products for the age of the aerosol reaching Svalbard indicate that, in general, aerosol in these events traveled faster compared to CS1 (See supplementary Figure S3), which agrees with the slightly lower SSA_{530} values observed.

By the late summer and early autumn, aerosol travel from lower latitudes to the Arctic is not as efficiently removed along the pathways as earlier, leading to a more efficient transport of polluted air masses and therefore an increase of the aerosol scattering and absorption coefficients measured (Gilardoni et al., 2023; Garrett et al., 2011). In addition, Pulimeno et al. (2024) showed an evident change of atmospheric transport regime in the summer of 2019, from North America during the summer period to North Europe and Russia during autumn and early-winter, which supports the anthropogenic origin of the aerosol measured during these events.

https://doi.org/10.5194/egusphere-2025-3423
Preprint. Discussion started: 15 September 2025

3.3 Aerosol radiative impact

Figure 12 presents the times series of anomaly of DNI (Δ_{DNI}) from June to September 2019 calculated as described in Section 3.3; only the cloud-free cases are used, selected depending on the value of the diffuse ratio (DifR) described. The adjacent years, 2018 and 2020, are also shown.

Despite the large amount of data with cloudy conditions (gaps in temporal series in Figure 12), all cloud-free cases presented negative Δ_{DNI} values in 2019 since 5 July, which can be explained by a smaller amount of DNI in 2019 due to the high aerosol load. Compared to the previous and next year, the Δ_{DNI} average in July-August 2019 was more than four times larger (negative sign), with a mean value of -73.6 W m^{-2}. In September, anomalies close to zero are observed, likely due to the reduced radiation received towards the end of the light season. The large standard deviation observed shows the complexity of this analysis, with multiple conditions (mainly variation in aerosols and clouds) sometimes playing roles in opposite directions. However, in general, the negative sign of Δ_{DNI} is a good proxy for the effect of the decrease in the direct component of solar radiation.

4 Conclusions

In order to understand the events leading to the high aerosol optical depth (AOD) and back-scatter values observed during the summer of 2019 (June to September), all available observational data in Spitsbergen, together with FLEXPART calculations, have been combined in this study. As a result, it was found that we faced multiple aerosol sources.

The present analysis revealed that the aerosols in Svalbard in the summer of 2019 reached the troposphere and also the stratosphere. However, these periods of high AOD were perceived differently by the remote sensing and in-situ instruments. In the remote sensing instruments (atmospheric column) the whole summer from mid July till end of September showed slightly variable but continuous unusual high AOD. Three events in the atmospheric column were identified: 6 to 11 July, CS1, 26 to 30 July, C2, and 6 to 19 August, C3. Contrary, the in-situ stations records were not remarkable except for three surface events: 5 to 9 July, CS1, 30 August, S1, and 12 September, S2, which showed high aerosol scattering and absorption coefficients at surface level. Only the first event (CS1) was observed simultaneously at the surface and at elevations up to 4000, suggesting that most of the aerosol during this summer was advected above the boundary layer. Due to cloudy conditions, remote sensing observations were not possible during S1 and S2.

The correlation of aerosol absorption and scattering coefficients between the two nearby in-situ sites used for the study was relatively weak (Pearson coefficient of 0.71 and 0.34, respectively), indicating that the deposition of aerosol in Ny-Ålesund might be dominated by local micrometeorological processes. Therefore it is useful to considerate both stations for comparison with climate models and long-range transport.

The aerosol properties from sun-photometer and lidar fairly agrees. Accumulation mode particles (around 0.1μm) were found mostly in the troposphere, and a weaker Accumulation mode of larger particles (around 0.2 μm) was observed mainly in the stratosphere. This second maximum was not found in the aerosol size distributions from mid-July when the first particles from the Raikoke volcano arrived to Ny-Ålesund. This might indicate the intrusion of some particles in the stratosphere,

https://doi.org/10.5194/egusphere-2025-3423
Preprint. Discussion started: 15 September 2025

however, no lidar measurements were available in July in order to corroborate it. Some big particles, which may had grown hygroscopically over water (as they maintained their weak depolarization), were also observed. Coarse mode particles were very sparse, as expected after long range transport.

The backward analysis of airmasses using FLEXPART has been useful to shed light on the origin of the aerosol, identifying three different sources: Raikoke volcano, biomass burning (BB) events and anthropogenic pollution. The modelled BC concentrations agrees with AOD values measured with the sun-photometer, correctly determining the intensity of each event. FLEXPART simulations indicated that the Raikoke volcano contributed until end of August to the AOD; however the remote sensing measurements showed a similar pattern in September than in the previous months, pointing out that probably remnants of the volcanic particles and also BB events stayed longer in the stratosphere. Further, different BB sources and different anthropogenic pollution sources were detected. Though the BB events occurred mainly between 500 and 4000 km a.g.l., some self-lifting might have occurred so that it reached the stratosphere, probably after even C2. Over the period from June to September, in the surface in-situ samplers, the BB and volcanic impact was minor, while anthropogenic emissions had more influence.

Despite its variable origin, this long-lasting summer episode of high AOD, consisted of spherical (low depolarization), weakly absorbing particles (high SSA), and small particles (Accumulation mode). As it occurred in late summer (relatively high solar altitude and low surface albedo), it contributed to a clear cooling signal; the anomaly of solar direct normal irradiance (Δ_{DNI}) was generally below -50 $\mathrm{W/m^2}$, with a mean of -73.6 $\mathrm{W/m^2}$ in July and August.

The analyses of the results obtained from various methods and climate models was not a trivial task. It is obvious that there is a strong need for dedicated campaigns to bring together all methods of AOD studies, including both the in situ and remote sensing ones. Ship born studies with in situ aerosol and Microtops II measurements facilitate very good study ground, especially, due to the fact that the ocean boundary layer is less disrupted than that over land, especially in the fjords, where aerosol studies can be affected by mountain orography (e.g. in Ny-Ålesund). In general, for the complete understanding of this long-lasting high AOD episode during summer 2019, the combination of the different instruments in and around Ny-Ålesund has been crucial, highlighting the importance of multi-instrumental studies and collaborations between different institutions and research areas.

Data availability. The AOD measurements can be found in Rehearsol https://doi.org/10.21343/1gaj-4645. Aerosol inversion properties can be downloaded at AERONET webpage: https://aeronet.gsfc.nasa.gov/. In-situ data for GAL associated with project RIS ID 3693: Gruvebadet Atmospheric Laboratory available under reques to the authors In-situ data for ZEP is available under request to the authors. CALIOP data can be found in http://www.icare.univ-lille1.fr/ KARL data is available under request to the authors. The radiation data can be found at Maturilli (2020) https://doi.org/10.1594/PANGAEA.914927. The results of the FLEXPART model simulations are openly available via https://atmo-access.nilu.no/ZEPP_lidar.py.

https://doi.org/10.5194/egusphere-2025-3423
Preprint. Discussion started: 15 September 2025

Author contributions. SHA and SaG conceived the main ideas of the study, developed the core concepts, and wrote the manuscript with input from all authors. SHA, DM, and RR contributed to the columnar aerosol measurements and their analysis. NK, SK, and TZ also contributed to the columnar aerosol measurements. SG, MM, DHR, and RK provided and processed the in-situ data. KS was responsible for the satellite data. SaG and CR developed the vertically-resolved aerosol properties analysis and handled the KARL data. NE and SE performed the FLEXPART simulations and conducted the modeling analysis. DM contributed to the radiative impact assessment. SHA, RR, DM, and SK secured funding for the study. All authors participated in scientific discussions and reviewed the manuscript

Competing interests. At least one of the (co-)authors is a member of the editorial board of Atmospheric Chemistry and Physics.

Acknowledgements. FLEXPART model simulations are cross-atmospheric research infrastructure services provided by ATMO-ACCESS (EU grant agreement No 101008004). The simulations were performed on resources provided by Sigma2 - the National Infrastructure for High Performance Computing and Data Storage in Norway. We thank NASA and CNES engineers and scientists for making CALIOP data available. We thank Piotr Sobolewski, Piotr Glowacki, Grzegorz Karasinski, Pawan Gupta, Elena Lind and their staff for establishing and maintaining the Hornsund site from AERONET used in this investigation. This work is part of the project TED2021-131211B-I00375 funded by MCIN/AEI/10.13039/501100011033 and European Union, "NextGenerationEU"/PRTR. This work was supported by the Ministerio de Ciencia e Innovacion (MICINN), with the grant no. PID2021-127588OB-I00 and is based on work from COST Action CA21119 HARMONIA. Financial support of the Department of Education, Junta de Castilla y León, and FEDER Funds is gratefully acknowledged (Reference: CLU-2023-1-05). The authors acknowledge the support of the Spanish Ministry for Science and Innovation to ACTRIS ERIC. Grant PID2022-142708NA-I00 funded by MCIN/AEI/10.13039/501100011033 is also acknowledged. The authors thank CNR and the staff of Dirigibile Italia for their support managing the Gruvebadet instrumentation. The authors would like to thank PAIGE (Italian-German Partnership) project.

https://doi.org/10.5194/egusphere-2025-3423
Preprint. Discussion started: 15 September 2025

References

Ansmann, A., Ohneiser, K., Chudnovsky, A., Baars, H., and Engelmann, R.: CALIPSO aerosol-typing scheme misclassified stratospheric fire smoke: Case study from the 2019 Siberian wildfire season, Frontiers in Environmental Science, 9, 769 852, 2021.

Ansmann, A., Veselovskii, I., Ohneiser, K., and Chudnovsky, A.: Comment on "Stratospheric Aerosol Composition Observed by the Atmospheric Chemistry Experiment Following the 2019 Raikoke Eruption" by Boone et al., Journal of Geophysical Research: Atmospheres, 129, e2022JD038 080, https://doi.org/10.1029/2022JD038080, 2024.

Böckmann, C., Ritter, C., and Graßl, S.: Improvement of Aerosol Coarse-Mode Detection through Additional Use of Infrared Wavelengths in the Inversion of Arctic Lidar Data, Remote Sensing, 16, 1576–1576, https://doi.org/10.3390/rs16091576, 2024.

Bond, T. C., Doherty, S. J., Fahey, D. W., Forster, P. M., Berntsen, T., DeAngelo, B. J., Flanner, M. G., Ghan, S., Kärcher, B., Koch, D., Kinne, S., Kondo, Y., Quinn, P. K., Sarofim, M. C., Schultz, M. G., Schulz, M., Venkataraman, C., Zhang, H., Zhang, S., Bellouin, N., Guttikunda, S. K., Hopke, P. K., Jacobson, M. Z., Kaiser, J. W., Klimont, Z., Lohmann, U., Schwarz, J. P., Shindell, D., Storelvmo, T., Warren, S. G., and Zender, C. S.: Bounding the role of black carbon in the climate system: A scientific assessment, Journal of Geophysical Research: Atmospheres, 118, 5380–5552, https://doi.org/10.1002/jgrd.50171, 2013.

Boone, C. D., Bernath, P. F., Labelle, K., and Crouse, J.: Stratospheric Aerosol Composition Observed by the Atmospheric Chemistry Experiment Following the 2019 Raikoke Eruption, Journal of Geophysical Research: Atmospheres, 127, e2022JD036 600, https://doi.org/10.1029/2022JD036600, e2022JD036600 2022JD036600, 2022.

Calì Quaglia, F., Meloni, D., Muscari, G., Di Iorio, T., Ciardini, V., Pace, G., Becagli, S., Di Bernardino, A., Cacciani, M., Hannigan, J. W., et al.: On the Radiative Impact of Biomass-Burning Aerosols in the Arctic: The August 2017 Case Study, Remote Sensing, 14, 313, 2022.

Cameron, W., Bernath, P., and Boone, C.: Sulfur dioxide from the atmospheric chemistry experiment (ACE) satellite, Journal of Quantitative Spectroscopy and Radiative Transfer, 258, 107 341, https://doi.org/10.1016/j.jqsrt.2020.107341, 2021.

CAMS: Another active year for Arctic wildfires, https://atmosphere.copernicus.eu/another-active-year-arctic-wildfires, accessed on 28 November 2024, 2020.

Cassiani, M., Stohl, A., and Brioude, J.: Lagrangian stochastic modelling of dispersion in the convective boundary layer with skewed turbulence conditions and a vertical density gradient: Formulation and implementation in the FLEXPART model, Boundary-Layer Meteorology, 154, 367–390, 2015.

Cheremisin, A., Marichev, V., Novikov, P., Pavlov, A., Shmirko, K., and Bochkovskii, D.: Assessing the transport of volcanic aerosol in the stratosphere over Tomsk and Vladivostok from lidar data, Russian Meteorology and Hydrology, 44, 345–354, 2019.

Dall'Osto, M., Beddows, D., Tunved, P., Harrison, R. M., Lupi, A., Vitale, V., Becagli, S., Traversi, R., Park, K.-T., Yoon, Y. J., et al.: Simultaneous measurements of aerosol size distributions at three sites in the European high Arctic, Atmospheric Chemistry and Physics, 19, 7377–7395, 2019.

Emde, C., Buras-Schnell, R., Kylling, A., Mayer, B., Gasteiger, J., Hamann, U., Kylling, J., Richter, B., Pause, C., Dowling, T., et al.: The libRadtran software package for radiative transfer calculations (version 2.0.1), Geoscientific Model Development, 9, 1647–1672, https://doi.org/10.5194/gmd-9-1647-2016, 2016.

Fazel-Rastgar, F. and Sivakumar, V.: Weather pattern associated with climate change during Canadian Arctic wildfires: A case study in July 2019, Remote Sensing Applications: Society and Environment, 25, 100 698, https://doi.org/10.1016/j.rsase.2022.100698, 2022.

Forster, C., Stohl, A., and Seibert, P.: Parameterization of Convective Transport in a Lagrangian Particle Dispersion Model and Its Evaluation, Journal of Applied Meteorology and Climatology, 46, 403 – 422, https://doi.org/10.1175/JAM2470.1, 2007.

https://doi.org/10.5194/egusphere-2025-3423
Preprint. Discussion started: 15 September 2025

Garrett, T. J., Brattström, S., Sharma, S., Worthy, D. E. J., and Novelli, P.: The role of scavenging in the seasonal transport of black carbon and sulfate to the Arctic, Geophysical Research Letters, 38, https://doi.org/10.1029/2011GL048221, 2011.

Gilardoni, S., Lupi, A., Mazzola, M., Cappelletti, D. M., Moroni, B., Ferrero, L., Markuszewski, P., Rozwadowska, A., Krejci, R., Zieger, P., et al.: Atmospheric black carbon in Svalbard (ABC Svalbard), SESS report, pp. 200–201, 2019.

Gilardoni, S., Heslin-Rees, D., Mazzola, M., Vitale, V., Sprenger, M., and Krejci, R.: Drivers controlling black carbon temporal variability in the lower troposphere of the European Arctic, Atmospheric Chemistry and Physics, 23, 15 589–15 607, https://doi.org/10.5194/acp-23-15589-2023, 2023.

González, R., Toledano, C., Román, R., Mateos, D., Asmi, E., Rodríguez, E., Lau, I. C., Ferrara, J., D'Elia, R., Antuña-Sánchez, J. C., et al.: Characterization of stratospheric smoke particles over the Antarctica by remote sensing instruments, Remote Sensing, 12, 3769, 2020.

Gorkavyi, N., Krotkov, N., Li, C., Lait, L., Colarco, P., Carn, S., DeLand, M., Newman, P., Schoeberl, M., Taha, G., et al.: Tracking aerosols and SO 2 clouds from the Raikoke eruption: 3D view from satellite observations, Atmospheric Measurement Techniques, 14, 7545–7563, 2021.

Graßl, S., Ritter, C., Wilsch, J., Herrmann, R., Doppler, L., and Román, R.: From Polar Day to Polar Night: A Comprehensive Sun and Star Photometer Study of Trends in Arctic Aerosol Properties in Ny-Ålesund, Svalbard, Remote Sensing, 16, 3725, https://doi.org/10.3390/rs16193725, 2024.

Graßl, S. and Ritter, C.: Properties of Arctic Aerosol Based on Sun Photometer Long-Term Measurements in Ny-Ålesund, Svalbard, Remote Sensing, 11, https://doi.org/10.3390/rs11111362, 2019.

Grythe, H., Kristiansen, N. I., Groot Zwaaftink, C. D., Eckhardt, S., Ström, J., Tunved, P., Krejci, R., and Stohl, A.: A new aerosol wet removal scheme for the Lagrangian particle model FLEXPART v10, Geoscientific Model Development, 10, 1447–1466, https://doi.org/10.5194/gmd-10-1447-2017, 2017.

Hansen, G., Kouremeti, N., Gilardoni, S., Stebel, K., Evangeliou, N., Ritter, C., Zielinski, T., Herrero, S., Kazadzis, S., Mateos, D., Mazzola, M., Pakszys, P., and Eleftheriadis, K.: Long-term observations of aerosol optical depth and their relation to in-situ aerosol properties in the Svalbard region (LOAD-RIS), https://doi.org/10.5281/zenodo.7376140, 2023.

Hansen, G. H., Zielinski, T., Pakszys, P., Ritter, C., Gilardoni, S., Eleftheriadis, K., Kouremeti, N., Mateos, D., Herrero, S., Kazadzis, S., et al.: Re-evaluation and Homogenization of Aerosol Optical Depth Observations in Svalbard (ReHearsol), RCN Project No: 311250/E40 - ReHearsol Final Report (NILU report 03/2022). Kjeller: NILU, 2022.

Herber, A., Thomason, L. W., Gernandt, H., Leiterer, U., Nagel, D., Schulz, K.-H., Kaptur, J., Albrecht, T., and Notholt, J.: Continuous day and night aerosol optical depth observations in the Arctic between 1991 and 1999, Journal of Geophysical Research: Atmospheres, 107, AAC 6–1–AAC 6–13, https://doi.org/10.1029/2001JD000536, 2002.

Hersbach, H., Bell, B., Berrisford, P., Hirahara, S., Horányi, A., Muñoz-Sabater, J., Nicolas, J., Peubey, C., Radu, R., Schepers, D., Simmons, A., Soci, C., Abdalla, S., Abellan, X., Balsamo, G., Bechtold, P., Biavati, G., Bidlot, J., Bonavita, M., De Chiara, G., Dahlgren, P., Dee, D., Diamantakis, M., Dragani, R., Flemming, J., Forbes, R., Fuentes, M., Geer, A., Haimberger, L., Healy, S., Hogan, R. J., Hólm, E., Janisková, M., Keeley, S., Laloyaux, P., Lopez, P., Lupu, C., Radnoti, G., de Rosnay, P., Rozum, I., Vamborg, F., Villaume, S., and Thépaut, J.-N.: The ERA5 global reanalysis, Quarterly Journal of the Royal Meteorological Society, 146, 1999–2049, https://doi.org/10.1002/qj.3803, 2020.

Hoffmann, A.: Comparative aerosol studies based on multi-wavelength Raman LIDAR at Ny-Ålesund, Spitsbergen, Ph.D. thesis, Universität Potsdam, 2011.

https://doi.org/10.5194/egusphere-2025-3423
Preprint. Discussion started: 15 September 2025

Holben, B. N., Eck, T. F., Slutsker, I., Tanré, D., Buis, J. P., Setzer, A., Vermote, E., Reagan, J. A., Kaufman, Y. J., Nakajima, T., Lavenu, F., Jankowiak, I., and Smirnov, A.: AERONET – a federated instrument network and data archive for aerosol characterization, Remote Sens. Environ., 66, 1–16, 1998.

Johnson, M. S., Strawbridge, K., Knowland, K. E., Keller, C., and Travis, M.: Long-range transport of Siberian biomass burning emissions to North America during FIREX-AQ, Atmospheric Environment, 252, 118 241, 2021.

Kaiser, J. W., Heil, A., Andreae, M. O., Benedetti, A., Chubarova, N., Jones, L., Morcrette, J.-J., Razinger, M., Schultz, M. G., Suttie, M., and van der Werf, G. R.: Biomass burning emissions estimated with a global fire assimilation system based on observed fire radiative power, Biogeosciences, 9, 527–554, https://doi.org/10.5194/bg-9-527-2012, 2012.

Kazadzis, S., Kouremeti, N., Nyeki, S., Gröbner, J., and Wehrli, C.: The World Optical Depth Research and Calibration Center (WORCC) quality assurance and quality control of GAW-PFR AOD measurements, Geoscientific Instrumentation, Methods and Data Systems, 7, 39–53, https://doi.org/10.5194/gi-7-39-2018, 2018.

Kharuk, V. I., Dvinskaya, M. L., Im, S. T., Golyukov, A. S., and Smith, K. T.: Wildfires in the Siberian Arctic, Fire, 5, https://doi.org/10.3390/fire5040106, 2022.

Klimont, Z., Kupiainen, K., Heyes, C., Purohit, P., Cofala, J., Rafaj, P., Borken-Kleefeld, J., and Schöpp, W.: Global anthropogenic emissions of particulate matter including black carbon, Atmospheric Chemistry and Physics, 17, 8681–8723, https://doi.org/10.5194/acp-17-8681-2017, 2017.

Kloss, C., Berthet, G., Sellitto, P., Ploeger, F., Taha, G., Tidiga, M., Eremenko, M., Bossolasco, A., Jégou, F., Renard, J.-B., et al.: Stratospheric aerosol layer perturbation caused by the 2019 Raikoke and Ulawun eruptions and their radiative forcing, Atmospheric Chemistry and Physics, 21, 535–560, 2021.

König-Langlo, G., Sieger, R., Schmithüsen, H., Bücker, A., Richter, F., and Dutton, E.: The baseline surface radiation network and its World radiation monitoring centre at the Alfred Wegener Institute, WCRP Report, WCRP-2, 2013.

Kouremeti, N., Kazadzis, S., Wehrli, C., Nyeki, S., Hansen, G. H., and Stebel, K.: WORCC-PMOD/WRC quality assured aerosol optical depth and Ångström exponent for Ny-Ålesund GAW station (2002 - present), https://doi.org/10.5281/zenodo.7191072, 2022.

Law, K. S. and Stohl, A.: Arctic air pollution: Origins and impacts, science, 315, 1537–1540, 2007.

Lisok, J., Rozwadowska, A., Pedersen, J. G., Markowicz, K. M., Ritter, C., Kaminski, J. W., Struzewska, J., Mazzola, M., Udisti, R., Becagli, S., et al.: Radiative impact of an extreme Arctic biomass-burning event, Atmospheric Chemistry and Physics, 18, 8829–8848, 2018.

Liu, S., Aiken, A. C., Arata, C., Dubey, M. K., Stockwell, C. E., Yokelson, R. J., Stone, E. A., Jayarathne, T., Robinson, A. L., DeMott, P. J., et al.: Aerosol single scattering albedo dependence on biomass combustion efficiency: Laboratory and field studies, Geophysical Research Letters, 41, 742–748, 2014.

Long, C., George, A., Mace, G., and Ackerman, T.: A simple formula for determining Globally Clear Skies, in: Proceedings of the Fifth Atmospheric Radiation Measurement (ARM) Science Team Meeting: March 19-23, 1995, San Diego, California, p. 173, The Department, 1995.

Long, C. M., Nascarella, M. A., and Valberg, P. A.: Carbon black vs. black carbon and other airborne materials containing elemental carbon: Physical and chemical distinctions, Environmental Pollution, 181, 271–286, https://doi.org/10.1016/j.envpol.2013.06.009, 2013.

Markowicz, K. M., Zieliński, T., Blindheim, S., Gausa, M., Jagodnicka, A. K., Kardas, A. E., Kumala, W., Malinowski, S. P., Petelski, T., Posyniak, M., et al.: Study of vertical structure of aerosol optical properties with sun photometers and ceilometer during the MACRON campaign in 2007, Acta Geophysica, 60, 1308–1337, 2012.

https://doi.org/10.5194/egusphere-2025-3423
Preprint. Discussion started: 15 September 2025

Maturilli, M.: Basic and other measurements of radiation at station Ny-Ålesund (2006-05 et seq), https://doi.org/10.1594/PANGAEA.914927, 2020.

Maturilli, M., Herber, A., and König-Langlo, G.: Surface radiation climatology for Ny-Ålesund, Svalbard (78.9 N), basic observations for trend detection, Theoretical and Applied Climatology, 120, 331–339, 2015.

Mayer, B. and Kylling, A.: The libRadtran software package for radiative transfer calculations-description and examples of use, Atmospheric Chemistry and Physics, 5, 1855–1877, https://doi.org/10.5194/acp-5-1855-2005, 2005.

Mazzola, M., Stone, R., Herber, A., Tomasi, C., Lupi, A., Vitale, V., Lanconelli, C., Toledano, C., Cachorro, V., O'Neill, N., Shiobara, M., Aaltonen, V., Stebel, K., Zielinski, T., Petelski, T., Ortiz de Galisteo, J., Torres, B., Berjon, A., Goloub, P., Li, Z., Blarel, L., Abboud, I., Cuevas, E., Stock, M., Schulz, K.-H., and Virkkula, A.: Evaluation of sun photometer capabilities for retrievals of aerosol optical depth at high latitudes: The POLAR-AOD intercomparison campaigns, Atmospheric Environment, 52, 4–17, https://doi.org/10.1016/j.atmosenv.2011.07.042, physical, chemical, optical and radiative properties of polar aerosols – IPY 2007 - 2008, 2012.

McKee, K., Smith, C. M., Reath, K., Snee, E., Maher, S., Matoza, R. S., Carn, S., Mastin, L., Anderson, K., Damby, D., Roman, D. C., Degterev, A., Rybin, A., Chibisova, M., Assink, J. D., de Negri Leiva, R., and Perttu, A.: Evaluating the state-of-the-art in remote volcanic eruption characterization Part I: Raikoke volcano, Kuril Islands, Journal of Volcanology and Geothermal Research, 419, 107 354, https://doi.org/10.1016/j.jvolgeores.2021.107354, 2021.

Moholdt, G., Wesselink, D., and Aas, H. F.: Merged Svalbard digital terrain model, https://doi.org/10.21334/NPOLAR.2019.675565F7, 2019.

Morys, M., Mims III, F. M., Hagerup, S., Anderson, S. E., Baker, A., Kia, J., and Walkup, T.: Design, calibration, and performance of MICROTOPS II handheld ozone monitor and Sun photometer, Journal of Geophysical Research: Atmospheres, 106, 14 573–14 582, 2001.

Ohneiser, K., Ansmann, A., Chudnovsky, A., Engelmann, R., Ritter, C., Veselovskii, I., Baars, H., Gebauer, H., Griesche, H., Radenz, M., et al.: The unexpected smoke layer in the High Arctic winter stratosphere during MOSAiC 2019–2020, Atmospheric Chemistry and Physics, 21, 15 783–15 808, 2021.

Ohneiser, K., Ansmann, A., Witthuhn, J., Deneke, H., Chudnovsky, A., Walter, G., and Senf, F.: Self-lofting of wildfire smoke in the troposphere and stratosphere: simulations and space lidar observations, Atmospheric Chemistry and Physics, 23, 2901–2925, 2023.

Osborne, M. J., de Leeuw, J., Witham, C., Schmidt, A., Beckett, F., Kristiansen, N., Buxmann, J., Saint, C., Welton, E. J., Fochesatto, J., Gomes, A. R., Bundke, U., Petzold, A., Marenco, F., and Haywood, J.: The 2019 Raikoke volcanic eruption – Part 2: Particle-phase dispersion and concurrent wildfire smoke emissions, Atmospheric Chemistry and Physics, 22, 2975–2997, https://doi.org/10.5194/acp-22-2975-2022, 2022.

Pisso, I., Sollum, E., Grythe, H., Kristiansen, N. I., Cassiani, M., Eckhardt, S., Arnold, D., Morton, D., Thompson, R. L., Groot Zwaaftink, C. D., Evangeliou, N., Sodemann, H., Haimberger, L., Henne, S., Brunner, D., Burkhart, J. F., Fouilloux, A., Brioude, J., Philipp, A., Seibert, P., and Stohl, A.: The Lagrangian particle dispersion model FLEXPART version 10.4, Geoscientific Model Development, 12, 4955–4997, https://doi.org/10.5194/gmd-12-4955-2019, 2019.

Pulimeno, S., Bruschi, F., Feltracco, M., Mazzola, M., Gilardoni, S., Crocchianti, S., Cappelletti, D., Gambaro, A., and Barbaro, E.: Investigating the Presence of Biomass Burning Events at Ny-Ålesund: Optical and Chemical Insights from Summer-Fall 2019, Atmospheric Environment, 320, 120 336, 2024.

https://doi.org/10.5194/egusphere-2025-3423
Preprint. Discussion started: 15 September 2025

Rantanen, M., Karpechko, A. Y., Lipponen, A., Nordling, K., Hyvärinen, O., Ruosteenoja, K., Vihma, T., and Laaksonen, A.: The Arctic has warmed nearly four times faster than the globe since 1979, Communications earth & environment, 3, 168, 2022.

Rinaldi, M., Hiranuma, N., Santachiara, G., Mazzola, M., Mansour, K., Paglione, M., Rodriguez, C. A., Traversi, R., Becagli, S., Cappelletti, D., and Belosi, F.: Ice-nucleating particle concentration measurements from Ny-Ålesund during the Arctic spring–summer in 2018, Atmospheric Chemistry and Physics, 21, 14 725–14 748, https://doi.org/10.5194/acp-21-14725-2021, 2021.

Schmale, J., Zieger, P., and Ekman, A. M.: Aerosols in current and future Arctic climate, Nature Climate Change, 11, 95–105, 2021.

Schmale, J., Sharma, S., Decesari, S., Pernov, J., Massling, A., Hansson, H.-C., von Salzen, K., Skov, H., Andrews, E., Quinn, P. K., Upchurch, L. M., Eleftheriadis, K., Traversi, R., Gilardoni, S., Mazzola, M., Laing, J., and Hopke, P.: Pan-Arctic seasonal cycles and long-term trends of aerosol properties from 10 observatories, Atmospheric Chemistry and Physics, 22, 3067–3096, https://doi.org/10.5194/acp-22-3067-2022, 2022.

Serreze, M. C. and Barry, R. G.: Processes and impacts of Arctic amplification: A research synthesis, Global and planetary change, 77, 85–96, 2011.

Shupe, M. D., Rex, M., Blomquist, B., Persson, P. O. G., Schmale, J., Uttal, T., Althausen, D., Angot, H., Archer, S., Bariteau, L., et al.: Overview of the MOSAiC expedition: Atmosphere, Elem Sci Anth, 10, 00 060, 2022.

Sinyuk, A., Holben, B. N., Eck, T. F., Giles, D. M., Slutsker, I., Korkin, S., Schafer, J. S., Smirnov, A., Sorokin, M., and Lyapustin, A.: The AERONET Version 3 aerosol retrieval algorithm, associated uncertainties and comparisons to Version 2, Atmospheric Measurement Techniques, 13, 3375–3411, 2020.

Smirnov, A., Holben, B., Slutsker, I., Giles, D., McClain, C., Eck, T., Sakerin, S., Macke, A., Croot, P., Zibordi, G., et al.: Maritime aerosol network as a component of aerosol robotic network, Journal of Geophysical Research: Atmospheres, 114, 2009.

Stohl, A., Forster, C., Frank, A., Seibert, P., and Wotawa, G.: Technical note: The Lagrangian particle dispersion model FLEXPART version 6.2, Atmospheric Chemistry and Physics, 5, 2461–2474, https://doi.org/10.5194/acp-5-2461-2005, 2005.

Tunved, P., Ström, J., and Krejci, R.: Arctic aerosol life cycle: linking aerosol size distributions observed between 2000 and 2010 with air mass transport and precipitation at Zeppelin station, Ny-Ålesund, Svalbard, Atmospheric Chemistry and Physics, 13, 3643–3660, 2013a.

Tunved, P., Ström, J., and Krejci, R.: Arctic aerosol life cycle: linking aerosol size distributions observed between 2000 and 2010 with air mass transport and precipitation at Zeppelin station, Ny-Ålesund, Svalbard, Atmospheric Chemistry and Physics, 13, 3643–3660, 2013b.

Vaughan, G., Wareing, D., and Ricketts, H.: Measurement Report: Lidar measurements of stratospheric aerosol following the 2019 Raikoke and Ulawun volcanic eruptions, Atmospheric Chemistry and Physics, 21, 5597–5604, 2021.

Voronova, O., Zima, A., Kladov, V., and Cherepanova, E.: Anomalous wildfires in Siberia in summer 2019, Izvestiya, Atmospheric and Oceanic Physics, 56, 1042–1052, 2020.

Warneke, C., Froyd, K., Brioude, J., Bahreini, R., Brock, C., Cozic, J., De Gouw, J., Fahey, D., Ferrare, R., Holloway, J., et al.: An important contribution to springtime Arctic aerosol from biomass burning in Russia, Geophysical Research Letters, 37, 2010.

Wendisch, M., Brückner, M., Crewell, S., Ehrlich, A., Notholt, J., Lüpkes, C., Macke, A., Burrows, J., Rinke, A., Quaas, J., et al.: Atmospheric and surface processes, and feedback mechanisms determining Arctic amplification: A review of first results and prospects of the (AC) 3 project, Bulletin of the American Meteorological Society, 104, E208–E242, 2023.

Willis, M. D., Leaitch, W. R., and Abbatt, J. P.: Processes Controlling the Composition and Abundance of Arctic Aerosol, Reviews of Geophysics, 56, 621–671, https://doi.org/10.1029/2018RG000602, 2018.

https://doi.org/10.5194/egusphere-2025-3423
Preprint. Discussion started: 15 September 2025

Winker, D. M., Vaughan, M. A., Omar, A., Hu, Y., Powell, K. A., Liu, Z., Hunt, W. H., and Young, S. A.: Overview of the CALIPSO Mission and CALIOP Data Processing Algorithms, Journal of Atmospheric and Oceanic Technology, 26, 2310 – 2323, https://doi.org/10.1175/2009JTECHA1281.1, 2009.

Wittmann, M., Groot Zwaaftink, C. D., Steffensen Schmidt, L., Guðmundsson, S., Pálsson, F., Arnalds, O., Björnsson, H., Thorsteinsson, T., and Stohl, A.: Impact of dust deposition on the albedo of Vatnajökull ice cap, Iceland, The Cryosphere, 11, 741–754, 2017.

Xian, P., Zhang, J., O'Neill, N. T., Reid, J. S., Toth, T. D., Sorenson, B., Hyer, E. J., Campbell, J. R., and Ranjbar, K.: Arctic spring and summertime aerosol optical depth baseline from long-term observations and model reanalyses – Part 2: Statistics of extreme AOD events, and implications for the impact of regional biomass burning processes, Atmospheric Chemistry and Physics, 22, 9949–9967, https://doi.org/10.5194/acp-22-9949-2022, 2022a.

Xian, P., Zhang, J., O'Neill, N. T., Toth, T. D., Sorenson, B., Colarco, P. R., Kipling, Z., Hyer, E. J., Campbell, J. R., Reid, J. S., and Ranjbar, K.: Arctic spring and summertime aerosol optical depth baseline from long-term observations and model reanalyses – Part 1: Climatology and trend, Atmospheric Chemistry and Physics, 22, 9915–9947, https://doi.org/10.5194/acp-22-9915-2022, 2022b.

Zielinski, T., Bolzacchini, E., Cataldi, M., Ferrero, L., Graßl, S., Hansen, G., Mateos, D., Mazzola, M., Neuber, R., Pakszys, P., et al.: Study of chemical and optical properties of biomass burning aerosols during long-range transport events toward the arctic in summer 2017, Atmosphere, 11, 84, 2020.

https://doi.org/10.5194/egusphere-2025-3423
Preprint. Discussion started: 15 September 2025

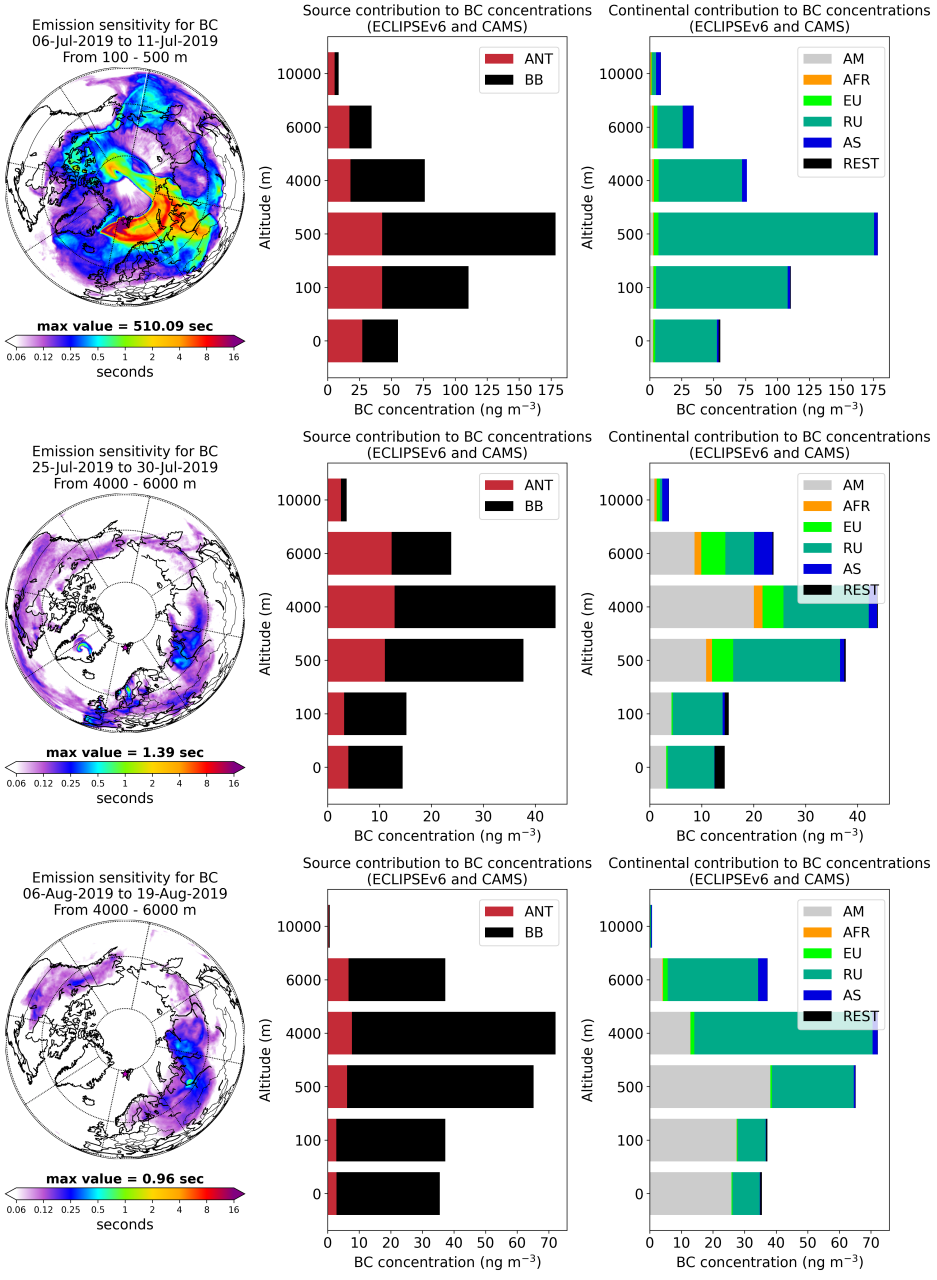

Figure 9. FLEXPART backward modeling results for the source regions of the airmasses arriving at ZEP Observatory: in top row from 6 to 11 July (CS1), in middle row from 26 to 30 July (C2) and in bottom row from 6 to 19 August (C3). On the right column it is shown the emission sensitivity for BC computed for the days of the events. The release height for the footprint is determined based on the altitude of maximum BC concentrations and is provided in the header. The modelled BC concentrations at five height levels (lower boundary: 0 m, 500 m, 4000 m, 6000 m and 10000 m) color-coded by source and continental contributions, are shown in the middle and right columns respectively. With respect the source we have distinguished between biomass burning (BB) and anthropogenic (ANT). For the region of origin, the labels used are: America (AM), Africa (AF), Europe (EU), Russia (RU), Asia (AS) and rest of the world (REST).

https://doi.org/10.5194/egusphere-2025-3423
Preprint. Discussion started: 15 September 2025

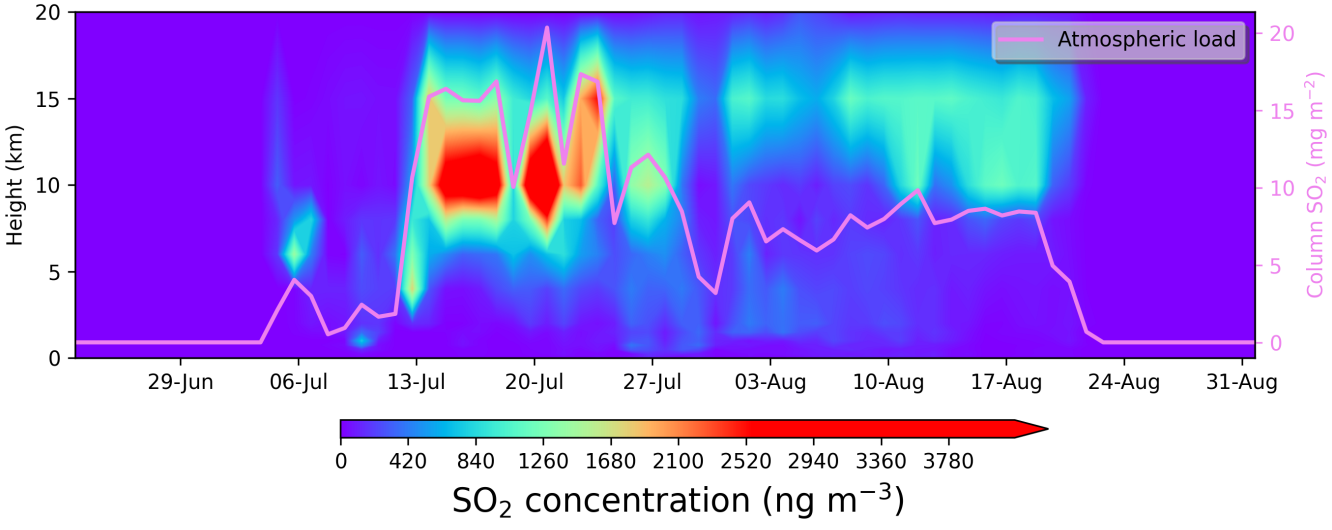

Figure 10. Time-height section of the volcanic SO_2 concentration (colored contours) as modelled by FLEXPART on its arrival at Ny-Ålesund station from end of June to end of August 2019. The red line indicates the modelled total column concentration.

https://doi.org/10.5194/egusphere-2025-3423
Preprint. Discussion started: 15 September 2025

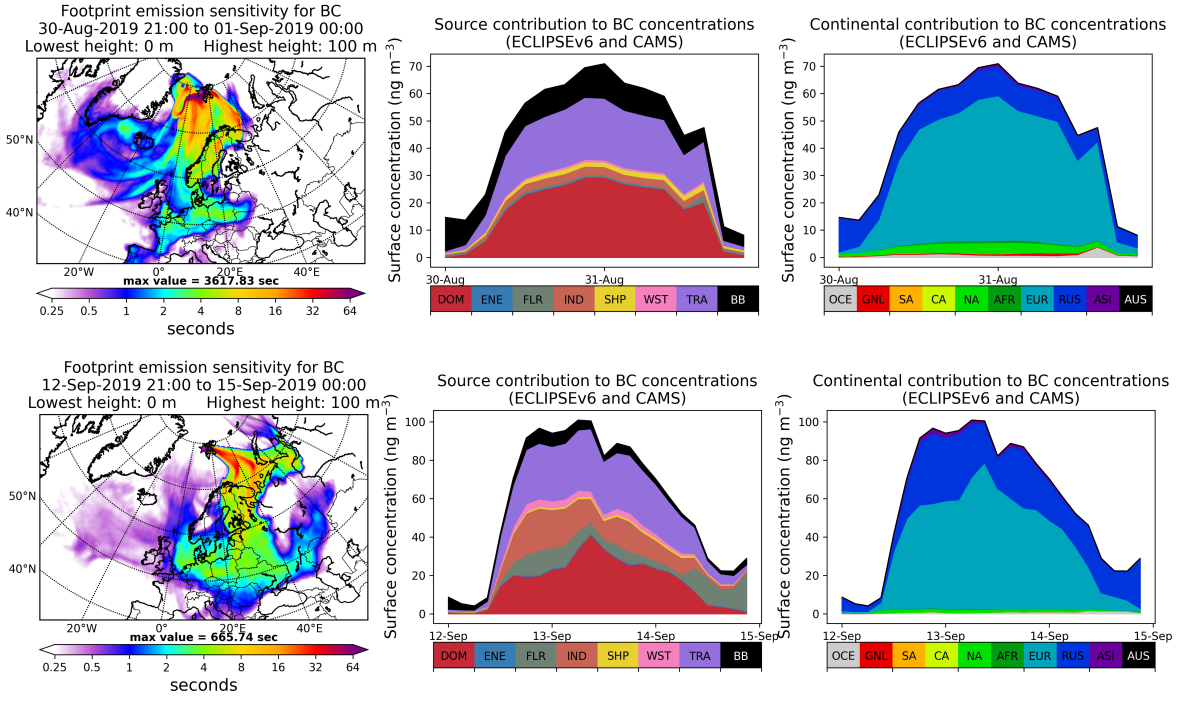

Figure 11. FLEXPART backward modeling results for the source regions of the airmasses arriving at ZEP Observatory during the enhanced pollution events on 30 August (S1, top row) and on 12 September (S2, bottom row). On the right column it is shown the emission sensitivity for BC computed for the days of the events. The temporal evolution of the modelled BC concentrations at the surface during the days of the events and days around, color-coded by source and continental contributions, are shown in the middle and right columns respectively. With respect the sources it has been distinguished between the biomass burning (BB) emissions and the following anthropogenic emissions: residential and commercial (DOM), energy production (ENE), gas flaring (FLR), industry (IND), shipping activities (SHP), waste treatment and disposal sector (WST) and transportation (TRA). For the region of origin the labels used are: America (AM), Africa (AF), Europe (EU), Russia (RU), Asia (AS) and rest of the world (REST).

https://doi.org/10.5194/egusphere-2025-3423
Preprint. Discussion started: 15 September 2025

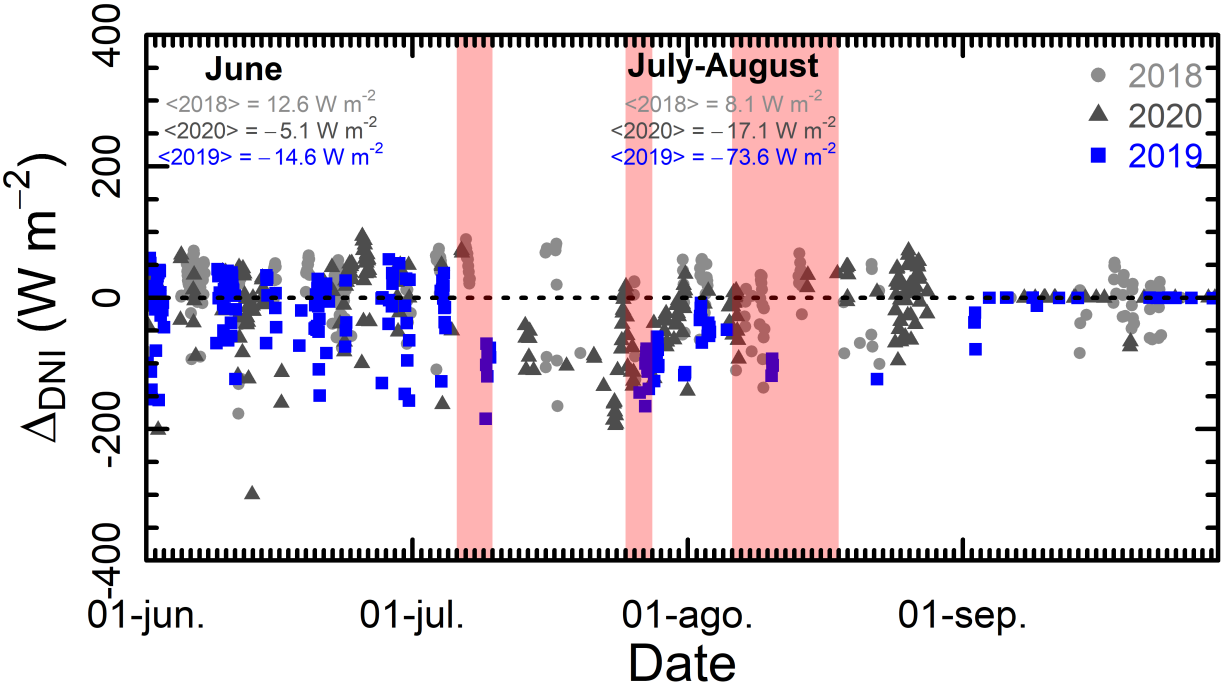

Figure 12. Anomaly of solar direct radiation in 2019, 2018 and 2020 with respect the reference value for the 2006-2020 period as described in Equation 2. The average anomaly of each year has been included in the left corner. The red shaded areas highlight the three columnar events analyzed throughout the study.